

A High–Order Perturbation of Surfaces Method for Vector Electromagnetic Scattering by Doubly Layered Periodic Crossed Gratings

Youngjoon Hong and David P. Nicholls

*Department of Mathematics, Statistics, and Computer Science,
University of Illinois at Chicago,
Chicago, IL, 60607 U.S.A.*

Abstract

The accurate simulation of scattering of electromagnetic waves in three dimensions by a diffraction grating is crucial in many applications of engineering and scientific interest. In this contribution we present a novel High–Order Perturbation of Surfaces method for the numerical approximation of vector electromagnetic scattering by a doubly periodic layered medium. For this we restate the governing time harmonic Maxwell equations as vector Helmholtz equations which are coupled by transmission boundary conditions at the layer interface. We then apply the method of Transformed Field Expansions which delivers a Fourier collocation, Legendre–Galerkin, Boundary Perturbation approach to solve the problem in transformed coordinates. A sequence of numerical simulations demonstrate the efficient and robust spectral convergence which can be achieved with the proposed algorithm.

Keywords: High–Order Spectral Methods, Vector Electromagnetic Scattering, Periodic Doubly Layered Media, High–Order Perturbation of Surfaces Methods

2000 MSC: 78A45, 65N35, 35J05, 41A58

Email address: `hongy@uic.edu`; `davidn@uic.edu` (Youngjoon Hong and David P. Nicholls)

¹ **1. Introduction**

² The accurate simulation of scattering of electromagnetic waves in three
³ dimensions by a diffraction grating is crucial in many applications of engi-
⁴ neering and scientific interest. Examples include surface enhanced Raman
⁵ scattering [XBKB99], extraordinary optical transmission [ELG⁺98], surface
⁶ enhanced spectroscopy [Mos85], photovoltaic devices [AP10], and surface
⁷ plasmon resonance biosensing [Hom08, LJJ⁺12]. Clearly, the ability to nu-
⁸ merically simulate such configurations with speed, accuracy, and robustness
⁹ is of the utmost importance to many disciplines. In this contribution we
¹⁰ present a novel High-Order Perturbation of Surfaces (HOPS) method for
¹¹ the numerical approximation of vector electromagnetic scattering by a peri-
¹² odic doubly layered medium.

¹³ Volumetric approaches to these problems are pervasive in the engineer-
¹⁴ ing literature. More specifically Finite Difference [LeV07], Finite Element
¹⁵ [Joh87], Discontinuous Galerkin [HW08], Spectral Element [DFM02], and
¹⁶ Spectral [GO77, STW11] methods are all widely used by practitioners. How-
¹⁷ ever, such methods are clearly disadvantaged with an unnecessarily large
¹⁸ number of unknowns for the piecewise homogeneous problems we consider
¹⁹ here. In addition, the faithful enforcement of outgoing wave conditions
²⁰ is problematic for these approaches typically necessitating approximations
²¹ such as the Perfectly Matched Layer [Bér94, Bér99] or exact, non-reflecting
²² boundary conditions [JN80, HW85, KG89, Giv99, NN04, BNNW09] which
²³ spoil the sparseness properties of the relevant linear systems.

²⁴ For these reasons, surface methods are an ideal choice as they are orders of
²⁵ magnitude faster when compared to volumetric approaches due to the greatly
²⁶ reduced number of degrees of freedom required to resolve a computation.
²⁷ In addition, far-field boundary conditions are enforced exactly through the
²⁸ choice of the Green function. Consequently, these methods are a very appeal-
²⁹ ing alternative which are gaining favor with practitioners. The most prevalent
³⁰ among these interfacial algorithms are those based upon Boundary Integral
³¹ Equations (BIEs) [CK13, RT04], but these face difficulties. Most have been
³² resolved in recent years through (i.) the use of sophisticated quadrature
³³ rules to deliver High-Order Spectral (HOS) accuracy; (ii.) the design of
³⁴ preconditioned iterative solvers with suitable acceleration [GR87]; (iii) new
³⁵ strategies to accelerate the convergence of the periodized Green function
³⁶ [BPA17, BLPAT16] (or avoiding its periodization entirely [BG11, CB15]);
³⁷ and (iv.) new approaches to deal with the Rayleigh singularities (widely

38 known in the literature as “Wood’s anomalies”) [BD14, BFL17, BSTV16].
39 As a result they are a compelling alternative for many problems of applied
40 interest, however, two properties render them disadvantaged for the *parameterized*
41 problems we consider as compared with the methods we advocate
42 here: (i.) For geometries specified by the real value, ε , (here the deviation of
43 the interface shapes from trivial), a BIE solver will provide a solution for a
44 single value of ε . If this is changed then the solver must be initiated again;
45 (ii.) the dense, non-symmetric positive definite systems of linear equations
46 that must be solved with each simulation. **As specific examples where such**
47 **considerations arise, we point the interested reader to the work of the second**
48 **author, F. Reitich, T. Johnson, and S.-H. Oh. on (i.) simulating “reflectivity**
49 **maps” associated to multilayer plasmonic devices [NRJO14] and (ii.)**
50 **determining the minimal configuration required to excite surface plasmons**
51 **with shallow gratings [NOJR16]. In the former, the parameterized nature of**
52 **the configuration and the associated reflectivity map would require a BIE to**
53 **be restarted with each new data point (unlike the scheme we advocate here).**
54 **In the latter, the geometry shape was, by design, a *very* small perturbation**
55 **of a flat-interface configuration. For a BIE method the cost of simulating**
56 **this is the same as that of approximating a grating with a large deformation,**
57 **while a perturbative algorithm (such as the one we discuss in this paper) can**
58 **run much more quickly.**

59 In contrast, a High-Order Perturbation of Surfaces (HOPS) methodology
60 effectively addresses these concerns. These formulations have the advantageous
61 properties of BIE formulations (e.g., surface formulation, reduced
62 numbers of degrees of freedom, and exact enforcement of far-field boundary
63 conditions) while being immune to the shortcomings listed above: (i.) Since
64 HOPS approaches are built upon expansions in the deformation parameter,
65 ε , once the Taylor coefficients are known for the problem unknowns, one
66 simply sums these for any choice of ε to recover the solution rather than
67 beginning a new simulation; (ii.) the perturbative nature of the scheme
68 is built upon the flat-interface solution which is trivially solved in Fourier
69 space by inverting a sparse operator at each wavenumber. We point out that
70 the initial smallness assumption on the deformation parameter, ε , can be
71 dropped in light of the analytic continuation results in [NR03, HN10] which
72 demonstrate that the domain of analyticity contains a neighborhood of the
73 *entire* real axis. Therefore, with appropriate numerical analytic continuation
74 methodologies (e.g., Padé approximation [BGM96]) to access this region of
75 analyticity, quite large and irregular perturbations can be simulated. We

76 direct the interested reader to [BR93b, BR94, BR01, NR01b, NR04b] for
77 numerical demonstrations.

78 There are several approaches to HOPS simulation of partial differen-
79 tial equations posed on irregular domains, but they all trace their begin-
80 nings to low-order calculations such as those of Rayleigh [Ray07] and Rice
81 [Ric51]. The first high-order incarnations appeared in the early 1990s with
82 the introduction of the methods of Operator Expansions (OE) by Milder
83 [Mil91a, Mil91b, MS91, MS92] and Field Expansions (FE) by Bruno and Re-
84 itich [BR93a, BR93b, BR93c]. Each has been enhanced by various authors,
85 but the most significant was the stabilization of these methods by one of
86 the authors and Reitich with the Transformed Field Expansions (TFE) al-
87 gorithm [NR01a, NR01b, NR03, NR04a, NR04b]. Beyond this, these HOPS
88 schemes have been extended in a number of directions. Of particular in-
89 terest to this contribution we mention bounded obstacle configurations
90 [BR98, NS06, FNS07], the full vector Maxwell equations [BR96, Nic15, NT16]
91 and a rigorous numerical analysis [NS09].

92 In addition to these, the authors have initiated a comprehensive study of
93 the TFE recursions for linear wave scattering and their extension to multiple
94 (three) layers in two dimensions [HN17b] and multiple (arbitrary numbers of)
95 layers in three dimensions [HN17a]. However, these investigations fixed upon
96 the scalar Helmholtz equations which only govern electromagnetic wave prop-
97 agation in two dimensions under Transverse Electric or Transverse Magnetic
98 polarization [Pet80]. In this contribution we examine the much more diffi-
99 cult problem of simulating electromagnetic radiation scattered by a crossed
100 grating in three dimensions in general polarization. This demands that we
101 not only solve the vector Helmholtz equations in three dimensions, but also
102 accommodate the more subtle interfacial boundary conditions of continuity
103 of tangential fields with appropriate jumps in the normal direction. To this
104 one must also add divergence free constraints while imposing appropriate
105 outgoing wave conditions to avoid pollution of solutions. We demonstrate
106 how this can be achieved in the doubly layered scenario for which the TFE
107 recursions have yet to be derived and implemented. Of particular note, we
108 describe a novel, spectrally accurate, modified Legendre–Galerkin approach
109 to the vertical discretization where the standard basis is enriched with addi-
110 tional connecting basis functions across the layer boundary.

111 In addition to the novelty of our new algorithm for this model, we also
112 point out that our approach will be the method of choice for simulating the
113 technologically relevant case of homogeneous layers separated by an interface

114 which is a slight to moderate deviation of flat. In this case volumetric ap-
 115 proaches will not be competitive due to their onerous operation counts and
 116 memory requirements, while BIE approaches (which have the same memory
 117 constraints as our TFE method) will take longer as their computational cost
 118 in this setting will be significantly greater. The combination of (i.) dense,
 119 non-symmetric positive-definite matrix inversion, and (ii.) the algorithmic
 120 and operational complications of evaluating the Green function (both its
 121 periodization and accounting for the Rayleigh singularities) render such ap-
 122 proaches non-competitive for the problems we consider here.

123 The article is organized as follows: In Section 2 the governing equations
 124 for linear electromagnetic waves interacting with a periodic doubly layered
 125 structure are carefully formulated, together with the appropriate interfacial
 126 boundary conditions. The TFE method is described in Section 3, and the
 127 modified Legendre-Galerkin scheme, which we implemented for the vertical
 128 discretization, is discussed in Sections 4 and 5. A sequence of numerical
 129 experiments are presented in Section 6 which demonstrate the stability and
 130 accuracy we can achieve in simulations of configurations containing not only
 131 smooth and small interfaces, but also rough and large ones as well.

132 2. Governing Equations

In this section we describe the governing equations of linear electromagnetic waves scattered by a doubly layered medium. Consider a grating structure with crossed periodic interface located at

$$z = g(x, y), \quad g(x + d_1, y + d_2) = g(x, y),$$

where z is the vertical coordinate, and x and y are the lateral coordinates. Dielectrics occupy each of the two domains

$$S_g^1 := \{z > g(x, y)\}, \quad S_g^2 := \{z < g(x, y)\},$$

with constant permittivities and permeabilities, $\{\epsilon_m, \mu_m\}$ ($m = 1, 2$), in each of the layers. The structure is illuminated from above by time-harmonic (with frequency ω) plane-wave incidence of the (reduced) form

$$\mathbf{H}^{\text{inc}} = \mathbf{A} e^{i(\alpha x + \beta y - \gamma z)}, \quad \nabla \cdot \mathbf{H}^{\text{inc}} = 0, \quad (1a)$$

$$\mathbf{E}^{\text{inc}} = \mathbf{B} e^{i(\alpha x + \beta y - \gamma z)}, \quad \nabla \cdot \mathbf{E}^{\text{inc}} = 0, \quad (1b)$$

where

$$\mathbf{A} \cdot (\alpha, \beta, -\gamma)^T = 0, \quad \mathbf{B} = -\frac{1}{i\omega\epsilon_1} \nabla \times \mathbf{A}.$$

¹³³ We follow the convention that bold-faced characters denote vectors and
¹³⁴ plain-faced are scalars, so that, for instance, $\mathbf{A} = (A^x, A^y, A^z)^T$.

In this setting electromagnetic radiation is governed by the time-harmonic forms of Faraday's and Ampere's Laws

$$\nabla \times \mathbf{E} - i\omega\mu\mathbf{H} = 0, \quad (2a)$$

$$\nabla \times \mathbf{H} + i\omega\epsilon\mathbf{E} = 0, \quad (2b)$$

respectively, which govern the reduced electric, \mathbf{E} , and magnetic, \mathbf{H} , fields. We consider $\mu = \mu_0$, the permeability of the vacuum, and the permittivity a piecewise constant

$$\epsilon = \begin{cases} \epsilon_1, & \text{in } S_g^1, \\ \epsilon_2, & \text{in } S_g^2. \end{cases}$$

¹³⁵ As there are no sources (current or charge), applying the divergence operator
¹³⁶ to (2) and using the fact that the divergence of a curl is zero, reveals Gauss'
¹³⁷ Law for Magnetism and Gauss' Law

$$\operatorname{div} [\mu_0\mathbf{H}] = 0, \quad \operatorname{div} [\epsilon\mathbf{E}] = 0, \quad (3)$$

¹³⁸ respectively, inside each layer. By applying the curl operator to (2) and using
¹³⁹ (3) one can see that each field satisfies the vector Helmholtz equations

$$\Delta\mathbf{E} + k^2\mathbf{E} = 0, \quad \Delta\mathbf{H} + k^2\mathbf{H} = 0, \quad (4)$$

where $k^2 = \omega^2\epsilon\mu$. We decompose the total magnetic and electric fields into reflected (layer 1) and transmitted (layer 2) components in the following way

$$\mathbf{E} = \begin{cases} \mathbf{E}_1 + \mathbf{E}^{\text{inc}}, & \text{in } S_g^1, \\ \mathbf{E}_2, & \text{in } S_g^2, \end{cases}, \quad \mathbf{H} = \begin{cases} \mathbf{H}_1 + \mathbf{H}^{\text{inc}}, & \text{in } S_g^1, \\ \mathbf{H}_2, & \text{in } S_g^2, \end{cases}$$

¹⁴⁰ and note that each of the $\{\mathbf{E}_m, \mathbf{H}_m\}$ also satisfy the vector Helmholtz equations, (4).

At this point we remark that it is sufficient to solve for the magnetic fields, \mathbf{H}_m , as the electric fields, \mathbf{E}_m , can be recovered from (2b),

$$\mathbf{E}_m = -\frac{1}{i\omega\epsilon_m} \nabla \times \mathbf{H}_m.$$

¹⁴² We could, of course, select the electric field as our unknown and recover
¹⁴³ the magnetic field from (2a). However, as we shall see, the magnetic field
¹⁴⁴ enjoys better smoothness properties across the grating interface (its normal
¹⁴⁵ component is continuous) than the electric field.

With this choice we select (4) as the governing equations for our unknowns \mathbf{H}_m in the bulk and now must specify boundary conditions for these. First, the periodicity of the grating interface demands quasiperiodicity of the fields, [Pet80],

$$\mathbf{H}_m(x + d_1, y + d_2, z) = e^{i\alpha d_1 + i\beta d_2} \mathbf{H}_m(x, y, z).$$

¹⁴⁶ Additionally, the scattered fields must be “outgoing” (upward propagating in
¹⁴⁷ S_g^1 and downward propagating in S_g^2) which we make precise in Section 2.1.

For interfacial boundary conditions, an application of Stokes’ Theorem to (2a) and (2b) yields the continuity of *tangential* components of the electric and magnetic fields in the absence of interface sources (currents and charges)

$$\mathbf{N} \times (\mathbf{E}_1 + \mathbf{E}^{\text{inc}} - \mathbf{E}_2) = 0, \quad \text{at } \Gamma, \quad (5a)$$

$$\mathbf{N} \times (\mathbf{H}_1 + \mathbf{H}^{\text{inc}} - \mathbf{H}_2) = 0, \quad \text{at } \Gamma, \quad (5b)$$

where $\mathbf{N} = (-\partial_x g, -\partial_y g, 1)^T$ is an upward pointing normal and Γ denotes the interface

$$\Gamma := \{(x, y, z) \mid z = g(x, y)\}.$$

¹⁴⁸ Using (2b), the first of these, (5a), can be written in terms of the magnetic
¹⁴⁹ field as

$$\mathbf{N} \times (\nabla \times \mathbf{H}_1 + \nabla \times \mathbf{H}^{\text{inc}} - \tau \nabla \times \mathbf{H}_2) = 0, \quad \text{at } \Gamma, \quad (6)$$

where

$$\tau := \frac{\epsilon_1}{\epsilon_2} = \frac{k_1^2}{k_2^2}.$$

The divergence theorem applied to (3) delivers the jump relations in the *normal* components of the fields

$$\mathbf{N} \cdot (\epsilon_1 \mathbf{E}_1 + \epsilon_1 \mathbf{E}^{\text{inc}} - \epsilon_2 \mathbf{E}_2) = 0, \quad \text{at } \Gamma, \quad (7a)$$

$$\mathbf{N} \cdot (\mathbf{H}_1 + \mathbf{H}^{\text{inc}} - \mathbf{H}_2) = 0, \quad \text{at } \Gamma, \quad (7b)$$

¹⁵⁰ where we have used $\mu = \mu_0$ to simplify the latter. From these we discover that
¹⁵¹ the change in permittivity across Γ induces a jump in the normal component

152 of the electric field, while the constant value of the permeability yields a
 153 magnetic field with continuous normal component.

154 However, as noted in [CF91], there is redundancy in these conditions so we
 155 appeal to the work of [KN99, JWP96] who demonstrate that for a sufficiently
 156 regular interface (Lipschitz continuous is smooth enough) the divergence free
 157 conditions in the bulk, (3), can be guaranteed by simply enforcing them at
 158 the interface

$$\operatorname{div} [\epsilon_m \mathbf{E}_m] = 0, \quad \operatorname{div} [\mathbf{H}_m] = 0, \quad \text{at } \Gamma. \quad (8)$$

159 We have now presented eight interfacial boundary conditions, but six should
 160 suffice for the six unknowns in (4). For our developments we find it most
 161 convenient to select (5b), (6), (7b), and the *difference* of the latter equation
 162 in (8) between \mathbf{H}_1 and \mathbf{H}_2 .

Gathering all of these equations, we now focus on the following problem

$$\Delta \mathbf{H}_1 + k_1^2 \mathbf{H}_1 = 0, \quad \text{in } S_g^1, \quad (9a)$$

$$\Delta \mathbf{H}_2 + k_2^2 \mathbf{H}_2 = 0, \quad \text{in } S_g^2, \quad (9b)$$

$$\mathbf{N} \times (\mathbf{H}_1 - \mathbf{H}_2) = -\mathbf{N} \times \mathbf{H}^{\text{inc}}, \quad \text{at } \Gamma, \quad (9c)$$

$$\mathbf{N} \cdot (\mathbf{H}_1 - \mathbf{H}_2) = -\mathbf{N} \cdot \mathbf{H}^{\text{inc}}, \quad \text{at } \Gamma, \quad (9d)$$

$$\mathbf{N} \times (\nabla \times \mathbf{H}_1 - \tau \nabla \times \mathbf{H}_2) = -\mathbf{N} \times \nabla \times \mathbf{H}^{\text{inc}}, \quad \text{at } \Gamma, \quad (9e)$$

$$\operatorname{div} [\mathbf{H}_1] - \operatorname{div} [\mathbf{H}_2] = 0, \quad \text{at } \Gamma, \quad (9f)$$

$$\text{OWC}[\mathbf{H}_1] = 0, \quad z \rightarrow \infty, \quad (9g)$$

$$\text{OWC}[\mathbf{H}_2] = 0, \quad z \rightarrow -\infty, \quad (9h)$$

163 where “OWC” stands for the outgoing (upward/downward propagating) wave
 164 condition which we make precise presently [Are09].

165

166 **Remark 1.** *An inspection of the mathematically careful literature shows that*
 167 *while our formulation is largely standard, the appearance of two of our surface*
 168 *conditions, (9d) and (9f), while true, are somewhat unusual. However, a*
 169 *more careful reading of these papers typically reveals that the bulk divergence-*
 170 *free conditions (3), or their surface versions (8), are used in rather subtle*
 171 *and implicit ways at important points of the analysis. One of our goals in*
 172 *this work is to make all of this explicit in the problem statement with a view*
 173 *towards efficient and high-order numerical simulation (rather than rigorous*
 174 *analysis). Our choice was one of many we could have made, and it was*
 175 *simply the one most convenient for our implementation.*

176 *2.1. Transparent Boundary Conditions*

The usual procedure when implementing the TFE method is to truncate the unbounded problem domain to a bounded one using a transparent (non-reflecting) boundary condition. For this we introduce artificial boundaries above and below the structure, and enforce boundary conditions to solve (9) equivalently. Introducing the planes

$$z = a > |g|_{L^\infty}, \quad z = b < -|g|_{L^\infty},$$

we define the domains

$$\begin{aligned} S^a &:= \{z > a\}, & S^b &:= \{z < b\}, \\ S_g^{1,a} &:= \{g(x, y) < z < a\}, & S_g^{2,b} &:= \{b < z < g(x, y)\}; \end{aligned}$$

see, e.g., Figure 1. Transparent boundary conditions can be enforced with

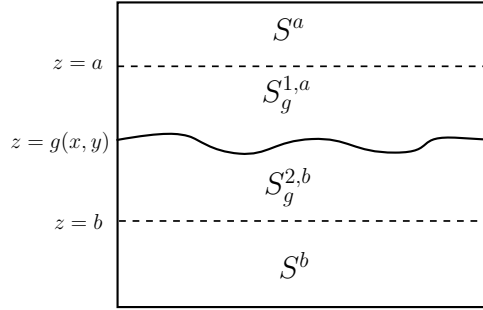


Figure 1: A depiction of the layered grating structure with artificial boundaries at $z = a$ and $z = b$.

Dirichlet–Neumann Operators (DNOs) from the Rayleigh expansions [Ray07] in the following way. More specifically, it is known [Pet80] that

$$\mathbf{H}_1(x, y, z) = \sum_{p=-\infty}^{\infty} \sum_{q=-\infty}^{\infty} \hat{\mathbf{t}}_{p,q} e^{i(\alpha_p x + \beta_q y + \gamma_{p,q}^{(1)}(z-a))}, \quad z > a,$$

and

$$\mathbf{H}_2(x, y, z) = \sum_{p=-\infty}^{\infty} \sum_{q=-\infty}^{\infty} \hat{\mathbf{s}}_{p,q} e^{i(\alpha_p x + \beta_q y + \gamma_{p,q}^{(2)}(b-z))}, \quad z < b,$$

where, for $p, q \in \mathbf{Z}$,

$$\alpha_p := \alpha + (2\pi/d_1)p, \quad \beta_q := \beta + (2\pi/d_2)q,$$

and

$$\gamma_{p,q}^{(m)} := \begin{cases} \sqrt{k_m^2 - \alpha_p^2 - \beta_q^2}, & (p, q) \in \mathcal{U}^m, \\ i\sqrt{\alpha_p^2 + \beta_q^2 - k_m^2}, & (p, q) \notin \mathcal{U}^m, \end{cases} \quad m = 1, 2,$$

and the set of propagating modes is

$$\mathcal{U}^m := \{p, q \in \mathbf{Z} \mid \alpha_p^2 + \beta_q^2 < k_m^2\}, \quad m = 1, 2.$$

It is not difficult to see that these solutions satisfy the Dirichlet conditions

$$\begin{aligned} \mathbf{H}_1(x, y, a) &= \sum_{p=-\infty}^{\infty} \sum_{q=-\infty}^{\infty} \hat{\mathbf{t}}_{p,q} e^{i(\alpha_p x + \beta_q y)} =: \mathbf{t}(x, y), \\ \mathbf{H}_2(x, y, b) &= \sum_{p=-\infty}^{\infty} \sum_{q=-\infty}^{\infty} \hat{\mathbf{s}}_{p,q} e^{i(\alpha_p x + \beta_q y)} =: \mathbf{s}(x, y). \end{aligned}$$

From these we can compute the Neumann data at the artificial boundaries,

$$\begin{aligned} \partial_z \mathbf{H}_1(x, y, a) &= \sum_{p=-\infty}^{\infty} \sum_{q=-\infty}^{\infty} (i\gamma_{p,q}^{(1)}) \hat{\mathbf{t}}_{p,q} e^{i(\alpha_p x + \beta_q y)}, \\ \partial_z \mathbf{H}_2(x, y, b) &= \sum_{p=-\infty}^{\infty} \sum_{q=-\infty}^{\infty} (-i\gamma_{p,q}^{(2)}) \hat{\mathbf{s}}_{p,q} e^{i(\alpha_p x + \beta_q y)}, \end{aligned}$$

and thus we define the DNOs

$$\begin{aligned} T_1[\mathbf{t}] &:= \sum_{p=-\infty}^{\infty} \sum_{q=-\infty}^{\infty} (i\gamma_{p,q}^{(1)}) \hat{\mathbf{t}}_{p,q} e^{i(\alpha_p x + \beta_q y)}, \\ T_2[\mathbf{s}] &:= \sum_{p=-\infty}^{\infty} \sum_{q=-\infty}^{\infty} (-i\gamma_{p,q}^{(2)}) \hat{\mathbf{s}}_{p,q} e^{i(\alpha_p x + \beta_q y)}, \end{aligned}$$

¹⁷⁷ which are order-one Fourier multipliers.

Using these DNOs at the artificial boundaries we write (9) *equivalently* on the bounded domain $\{b < z < a\}$,

$$\Delta \mathbf{H}_1 + k_1^2 \mathbf{H}_1 = 0, \quad \text{in } S_g^{1,a}, \quad (10a)$$

$$\Delta \mathbf{H}_2 + k_2^2 \mathbf{H}_2 = 0, \quad \text{in } S_g^{2,b}, \quad (10b)$$

$$\mathbf{N} \times (\mathbf{H}_1 - \mathbf{H}_2) = -\mathbf{N} \times \mathbf{H}^{\text{inc}}, \quad \text{at } \Gamma, \quad (10c)$$

$$\mathbf{N} \cdot (\mathbf{H}_1 - \mathbf{H}_2) = -\mathbf{N} \cdot \mathbf{H}^{\text{inc}}, \quad \text{at } \Gamma, \quad (10d)$$

$$\mathbf{N} \times (\nabla \times \mathbf{H}_1 - \tau \nabla \times \mathbf{H}_2) = -\mathbf{N} \times \nabla \times \mathbf{H}^{\text{inc}}, \quad \text{at } \Gamma, \quad (10e)$$

$$\text{div}[\mathbf{H}_1] - \text{div}[\mathbf{H}_2] = 0, \quad \text{at } \Gamma, \quad (10f)$$

$$\partial_z \mathbf{H}_1 - T_1[\mathbf{H}_1] = 0, \quad \text{at } z = a, \quad (10g)$$

$$\partial_z \mathbf{H}_2 - T_2[\mathbf{H}_2] = 0, \quad \text{at } z = b, \quad (10h)$$

¹⁷⁸ which are our governing equations.

¹⁷⁹ 3. Transformed Field Expansions

¹⁸⁰ We are now in a position to describe our TFE method. As always,
¹⁸¹ the algorithm begins with a domain flattening change of variables [NR01a]
¹⁸² (also known as σ -coordinates [Phi57] in the geophysical literature and the
¹⁸³ C-method [CMR80] in the electromagnetics community). Subsequently, a
¹⁸⁴ boundary perturbation expansion is conducted, resulting in a recurrently
¹⁸⁵ defined set of vector Helmholtz problems which must be solved at every per-
¹⁸⁶ turbation order desired.

¹⁸⁷ 3.1. The Change of Variables

To begin we define the change of variables

$$\begin{aligned} x' &= x, & y' &= y, \\ z_1 &= a \left(\frac{z - g}{a - g} \right), & g < z < a, & a > |g|_{L^\infty}, \\ z_2 &= b \left(\frac{g - z}{g - b} \right), & b < z < g, & b < -|g|_{L^\infty}, \end{aligned}$$

and the transformed fields

$$\mathbf{U}_m(x', y', z_m) := \mathbf{H}_m(x(x'), y(y'), z(x', y', z_m)), \quad m = 1, 2.$$

With this change of variables, a ponderous computation (see Appendix A) transforms (10) to the following system of equations

$$\Delta_1 \mathbf{U}_1 + k_1^2 \mathbf{U}_1 = \mathbf{R}_1, \quad \text{in } 0 < z_1 < a, \quad (11a)$$

$$\Delta_2 \mathbf{U}_2 + k_2^2 \mathbf{U}_2 = \mathbf{R}_2, \quad \text{in } b < z_2 < 0, \quad (11b)$$

$$[\![U^x]\!] = I_1, \quad \text{at } z_1 = z_2 = 0, \quad (11c)$$

$$[\![U^y]\!] = I_2, \quad \text{at } z_1 = z_2 = 0, \quad (11d)$$

$$[\![U^z]\!] = I_3, \quad \text{at } z_1 = z_2 = 0, \quad (11e)$$

$$[\![\partial_{x'} U^z]\!]_\tau - [\![(G/C) \partial_z U^x]\!]_\tau = Q_1, \quad \text{at } z_1 = z_2 = 0, \quad (11f)$$

$$[\![\partial_{y'} U^z]\!]_\tau - [\![(G/C) \partial_z U^y]\!]_\tau = Q_2, \quad \text{at } z_1 = z_2 = 0, \quad (11g)$$

$$[\![\partial_{x'} U^x]\!] + [\![\partial_{y'} U^y]\!] + \frac{a}{a-g} \partial_z U_1^z - \frac{b}{b-g} \partial_z U_2^z = J, \quad \text{at } z_1 = z_2 = 0, \quad (11h)$$

$$\partial_{z_1} \mathbf{U}_1 - T_1[\mathbf{U}_1] = \mathbf{B}_1, \quad \text{at } z_1 = a, \quad (11i)$$

$$\partial_{z_2} \mathbf{U}_2 - T_2[\mathbf{U}_2] = \mathbf{B}_2, \quad \text{at } z_2 = b, \quad (11j)$$

where

$$\mathbf{R}_m := \frac{1}{G_m^2} (\partial_{x'} R_m^x + \partial_{y'} R_m^y + \partial_{z_m} R_m^z + R_m^0), \quad m = 1, 2,$$

and

$$I_1 := -((\partial_{x'} g) A^z + A^x) \varphi - (\partial_{x'} g) [\![U^z]\!],$$

$$I_2 := -((\partial_{y'} g) A^z + A^y) \varphi - (\partial_{y'} g) [\![U^z]\!],$$

$$I_3 := ((\partial_{x'} g) A^x + (\partial_{y'} g) A^y - A^z) \varphi + (\partial_{x'} g) [\![U^x]\!] + (\partial_{y'} g) [\![U^y]\!],$$

$$\varphi := e^{(i\alpha x + i\beta y - i\gamma g(x, y))},$$

and

$$\begin{aligned} J &:= (\partial_{x'} g) \frac{a}{a-g} \partial_z U_1^x - (\partial_{x'} g) \frac{b}{b-g} \partial_z U_2^x \\ &\quad + (\partial_{y'} g) \frac{a}{a-g} \partial_z U_1^y - (\partial_{y'} g) \frac{b}{b-g} \partial_z U_2^y, \end{aligned}$$

$$\mathbf{B}_1 := -(g/a) T_1[\mathbf{U}_1],$$

$$\mathbf{B}_2 := -(g/b) T_2[\mathbf{U}_2],$$

and

$$[\![K]\!] := K_1 - K_2, \quad [\![K]\!]_\tau := K_1 - \tau K_2.$$

The Laplacian operator Δ_m is defined by

$$\Delta_m = \partial_{x'}^2 + \partial_{y'}^2 + \partial_{z_m}^2, \quad m = 1, 2.$$

188 We refer the reader to Appendix A for the specific formulas for the right
189 hand sides R_m^s and Q_m , (A.2) and (A.7), respectively.

190 *3.2. A High-Order Perturbation of Surfaces Method*

To specify our HOPS approach we consider an interface deformation of the form

$$g(x, y) = \varepsilon f(x, y), \quad \varepsilon \ll 1,$$

and insert this into the transformed equations (11). In a forthcoming publication it will be shown that the transformed fields depend *analytically* upon the parameter ε so that the following expansions are valid

$$\mathbf{U}_m = \sum_{n=0}^{\infty} \mathbf{U}_{m,n}(x, y, z) \varepsilon^n, \quad m = 1, 2.$$

From (11) we find at each perturbation order that

$$\Delta_1 \mathbf{U}_{1,n} + k_1^2 \mathbf{U}_{1,n} = \mathbf{R}_{1,n}, \quad \text{in } 0 < z_1 < a, \quad (12a)$$

$$\Delta_2 \mathbf{U}_{2,n} + k_2^2 \mathbf{U}_{2,n} = \mathbf{R}_{2,n}, \quad \text{in } b < z_2 < 0, \quad (12b)$$

$$[\![U_n^x]\!] = I_{1,n}, \quad \text{at } z_1 = z_2 = 0, \quad (12c)$$

$$[\![U_n^y]\!] = I_{2,n}, \quad \text{at } z_1 = z_2 = 0, \quad (12d)$$

$$[\![U_n^z]\!] = I_{3,n}, \quad \text{at } z_1 = z_2 = 0, \quad (12e)$$

$$[\![\partial_{x'} U_n^z]\!]_{\tau} - [\![\partial_z U_n^x]\!]_{\tau} = \tilde{Q}_{1,n}, \quad \text{at } z_1 = z_2 = 0, \quad (12f)$$

$$[\![\partial_{y'} U_n^z]\!]_{\tau} - [\![\partial_z U_n^y]\!]_{\tau} = \tilde{Q}_{2,n}, \quad \text{at } z_1 = z_2 = 0, \quad (12g)$$

$$[\![\partial_{x'} U_n^x]\!] + [\![\partial_{y'} U_n^y]\!] + [\![\partial_z U_n^z]\!] = \tilde{J}_n, \quad \text{at } z_1 = z_2 = 0, \quad (12h)$$

$$\partial_{z_1} \mathbf{U}_{1,n} - T_1[\mathbf{U}_{1,n}] = \mathbf{B}_{1,n}, \quad \text{at } z_1 = a, \quad (12i)$$

$$\partial_{z_2} \mathbf{U}_{2,n} - T_2[\mathbf{U}_{2,n}] = \mathbf{B}_{2,n}, \quad \text{at } z_2 = b. \quad (12j)$$

191 Again, we refer the reader to Appendix A for formulas for the right hand
192 sides $\mathbf{R}_{m,n}$, $I_{s,n}$, $\tilde{Q}_{m,n}$, \tilde{J}_n , and $\mathbf{B}_{m,n}$.

Considering the quasiperiodicity of solutions, we propose the following generalized Fourier (Floquet) series expansions

$$\{\mathbf{U}_{m,n}, \mathbf{R}_{m,n}\}(x, y, z) = \sum_{p=-\infty}^{\infty} \sum_{q=-\infty}^{\infty} \{\mathbf{U}_{m,n}^{p,q}, \mathbf{R}_{m,n}^{p,q}\}(z) e^{i(\alpha_p x + \beta_q y)},$$

$$\{I_{s,n}, \tilde{Q}_{m,n}, \tilde{J}_n, \mathbf{B}_{m,n}\}(x, y) = \sum_{p=-\infty}^{\infty} \sum_{q=-\infty}^{\infty} \{I_{s,n}^{p,q}, \tilde{Q}_{m,n}^{p,q}, \tilde{J}_n^{p,q}, \mathbf{B}_{m,n}^{p,q}\} e^{i(\alpha_p x + \beta_q y)}.$$

Inserting these expansions into (12), and using the fact that $(\gamma_{p,q}^{(m)})^2 = k_m^2 - \alpha_p^2 - \beta_q^2$, the governing equations are reduced to the one-dimensional boundary value problems

$$\partial_{z_1}^2 \mathbf{U}_{1,n}^{p,q} + (\gamma_{p,q}^{(1)})^2 \mathbf{U}_{1,n}^{p,q} = \mathbf{R}_{1,n}^{p,q}, \quad \text{in } 0 < z_1 < a, \quad (13a)$$

$$\partial_{z_2}^2 \mathbf{U}_{2,n}^{p,q} + (\gamma_{p,q}^{(2)})^2 \mathbf{U}_{2,n}^{p,q} = \mathbf{R}_{2,n}^{p,q}, \quad \text{in } b < z_2 < 0, \quad (13b)$$

$$[\![U_n^{x,p,q}]\!] = I_{1,n}^{p,q}, \quad \text{at } z_1 = z_2 = 0, \quad (13c)$$

$$[\![U_n^{y,p,q}]\!] = I_{2,n}^{p,q}, \quad \text{at } z_1 = z_2 = 0, \quad (13d)$$

$$[\![U_n^{z,p,q}]\!] = I_{3,n}^{p,q}, \quad \text{at } z_1 = z_2 = 0, \quad (13e)$$

$$i\alpha_p [\![U_n^{z,p,q}]\!]_{\tau} - [\![\partial_z U_n^{x,p,q}]\!]_{\tau} = \tilde{Q}_{1,n}^{p,q}, \quad \text{at } z_1 = z_2 = 0, \quad (13f)$$

$$i\beta_q [\![U_n^{z,p,q}]\!]_{\tau} - [\![\partial_z U_n^{y,p,q}]\!]_{\tau} = \tilde{Q}_{2,n}^{p,q}, \quad \text{at } z_1 = z_2 = 0, \quad (13g)$$

$$i\alpha_p [\![U_n^{x,p,q}]\!] + i\beta_q [\![U_n^{y,p,q}]\!] + [\![\partial_z U_n^{z,p,q}]\!] = \tilde{J}_n^{p,q}, \quad \text{at } z_1 = z_2 = 0, \quad (13h)$$

$$\partial_{z_1} \mathbf{U}_{1,n}^{p,q} - i\gamma_{p,q}^{(1)} \mathbf{U}_{1,n}^{p,q} = \mathbf{B}_{1,n}^{p,q}, \quad \text{at } z_1 = a, \quad (13i)$$

$$\partial_{z_2} \mathbf{U}_{2,n}^{p,q} + i\gamma_{p,q}^{(2)} \mathbf{U}_{2,n}^{p,q} = \mathbf{B}_{2,n}^{p,q}, \quad \text{at } z_2 = b. \quad (13j)$$

¹⁹³ We point out that the unique solvability of the full problem (9) [CF91, DF92,
¹⁹⁴ BF95] delivers a unique solution to (13).

¹⁹⁵ 4. Weak Formulation

In this section, we construct a weak formulation of (13) by decomposing solutions into two parts

$$\mathbf{U}_{m,n}^{p,q} = \tilde{\mathbf{U}}_{m,n}^{p,q} + \check{\mathbf{U}}_{m,n}^{p,q}, \quad m = 1, 2.$$

We choose the first term, $\tilde{\mathbf{U}}_{m,n}^{p,q}$, to solve (13) with $\mathbf{R}_{m,n}^{p,q}$ identically zero, and the second term, $\check{\mathbf{U}}_{m,n}^{p,q}$, to solve (13) with $I_{s,n}^{p,q}$, $\tilde{Q}_{m,n}^{p,q}$, $\tilde{J}_n^{p,q}$, and $\mathbf{B}_{m,n}^{p,q}$ all zero.

For the sake of simplicity we drop the indices $\{p, q, n\}$, and point out that it is not difficult to see that

$$\tilde{\mathbf{U}}_m = \mathbf{C}_m e^{i\gamma^{(m)} z} + \mathbf{D}_m e^{-i\gamma^{(m)} z}, \quad m = 1, 2,$$

where the coefficients

$$\mathbf{C}_m = (C_m^x, C_m^y, C_m^z)^T, \quad \mathbf{D}_m = (D_m^x, D_m^y, D_m^z)^T.$$

196 can be explicitly computed from the boundary conditions.

197 It remains to investigate the equations for $\tilde{\mathbf{U}}_m$ which can be solved by
198 a High-Order Spectral (HOS) method [STW11]. As both our Fourier
199 discretization of the lateral variables, (x, y) , and the Taylor approximation of
200 the perturbation quantity, ε , are spectrally accurate, it is natural to select
201 a HOS approach to discretize the vertical variable in order to maintain
202 high accuracy. Among HOS approaches, the Legendre-Galerkin methodology
203 [STW11] appealed to us due to its ease of implementation and stability
204 properties. We have used it in our previous work [HN17b, HN17a] and were
205 impressed with its performance; for this reason we have selected it again in
206 these developments.

However, we have not found the “standard” approaches appearing in the literature useful for our layered media problems and have devised our own “enriched” approach [HNS12, HN17b, HN17a]. To describe this we state that a classic weak formulation of (13) for $\tilde{\mathbf{U}}_m$ can be specified by: Find $\mathbf{V} \in [H^1([b, a])]^3$ such that

$$(\kappa^2 \mathbf{V}, \Phi) - (\partial_z \mathbf{V}, \partial_z \Phi) + (1 - \tau) \begin{pmatrix} \left(\partial_z \tilde{U}_2^x(0) - i\alpha_p \tilde{U}_2^z(0) \right) \bar{\varphi}^x(0) \\ \left(\partial_z \tilde{U}_2^y(0) - i\beta_q \tilde{U}_2^z(0) \right) \bar{\varphi}^y(0) \\ 0 \end{pmatrix} \\ = (\mathbf{R}, \Phi) - i\gamma^{(1)} \tilde{\mathbf{U}}_1(a) \bar{\Phi}(a) - i\gamma^{(2)} \tilde{\mathbf{U}}_2(b) \bar{\Phi}(b), \quad \forall \Phi \in [H^1([b, a])]^3,$$

where $I_1 := (0, a)$, $I_2 := (b, 0)$,

$$\{\mathbf{V}, \mathbf{R}, \kappa\} = \begin{cases} \{\tilde{\mathbf{U}}_1, \mathbf{R}_1, \gamma^{(1)}\}, & z \in I_1, \\ \{\tilde{\mathbf{U}}_2, \mathbf{R}_2, \gamma^{(2)}\}, & z \in I_2. \end{cases}$$

Here the vector pairing on the interval (a, b) is defined by

$$(\mathbf{u}, \mathbf{v}) := \int_a^b \begin{pmatrix} u_1 \bar{v}_1 \\ u_2 \bar{v}_2 \\ u_3 \bar{v}_3 \end{pmatrix} dx,$$

207 where the overbar denotes complex conjugation.

To construct a Legendre–Galerkin method as in [HN17b, HN17a], we define the finite–dimensional function space $\mathbf{X}_{N_z} \subset [H^1([(b, a)])]^3$ by

$$\mathbf{X}_{N_z} := \{\Phi_m \in [P_{N_y}(I_m)]^3 \mid \partial_z \Phi_1(a) - i\gamma^{(1)} \Phi_1(a) = 0, \\ \partial_z \Phi_2(b) + i\gamma^{(2)} \Phi_2(b) = 0, m = 1, 2\},$$

where P_{N_z} is the space of polynomials of degree less than N_z . The Legendre–Galerkin formulation is: Find $\mathbf{U}_{N_z} \in \mathbf{X}_{N_z}$ such that

$$(\kappa^2 \mathbf{U}_{N_z}, \Phi_{N_z}) - (\partial_z \mathbf{U}_{N_z}, \partial_z \Phi_{N_z}) \\ + (1 - \tau) \begin{pmatrix} \left(\partial_z \check{U}_{2,N_z}^x(0) - i\alpha_p \check{U}_{2,N_z}^z(0) \right) \bar{\varphi}_{N_z}^x(0) \\ \left(\partial_z \check{U}_{2,N_z}^y(0) - i\beta_q \check{U}_{2,N_z}^z(0) \right) \bar{\varphi}_{N_z}^y(0) \\ 0 \end{pmatrix} \\ = (\mathcal{I}_{N_z} \mathbf{R}, \Phi_{N_z}) - i\gamma^{(1)} \check{\mathbf{U}}_{N_z}(a) \bar{\Phi}_{N_z}(a) - i\gamma^{(2)} \check{\mathbf{U}}_{N_z}(b) \bar{\Phi}_{N_z}(b), \quad \forall \Phi_{N_z} \in \mathbf{X}_{N_z},$$

where \mathcal{I}_{N_z} is the projection operator onto P_{N_z} . Using integration by parts on each subdomain I_m , an equivalent variational formulation is derived: Find $\mathbf{U}_{N_z} \in \mathbf{X}_{N_z}$ such that

$$(\kappa^2 \mathbf{U}_{N_z}, \Phi_{N_z}) + (\partial_z^2 \mathbf{U}_{N_z}, \Phi_{N_z}) \\ + \begin{pmatrix} \left(\partial_z \check{U}_{1,N_z}^x(0) - \tau \partial_z \check{U}_{2,N_z}^x(0) - i\alpha_p (\check{U}_{1,N_z}^z(0) - \tau \check{U}_{2,N_z}^z(0)) \right) \bar{\varphi}_{N_z}^x(0) \\ \left(\partial_z \check{U}_{1,N_z}^y(0) - \tau \partial_z \check{U}_{2,N_z}^y(0) - i\beta_q (\check{U}_{1,N_z}^z(0) - \tau \check{U}_{2,N_z}^z(0)) \right) \bar{\varphi}_{N_z}^y(0) \\ \partial_z \left(\check{U}_{1,N_z}^z(0) - \check{U}_{2,N_z}^z(0) \right) \bar{\varphi}_{N_z}^z(0) \end{pmatrix} \\ = (\mathcal{I}_{N_z} \mathbf{R}, \Phi_{N_z}), \quad \forall \Phi_{N_z} \in \mathbf{X}_{N_z}.$$

208 **5. A Legendre–Galerkin Numerical Method in Enriched Spaces**

To apply the spectral Legendre–Galerkin approach [She94, STW11] we consider basis functions which are combinations of Legendre polynomials $L_j(z)$. For $z \in I_1$, we define

$$\psi_{1,j}^s(z) := (1 + i)L_j \left(\frac{2z - a}{a} \right) + a_{1,j} L_{j+1} \left(\frac{2z - a}{a} \right) \\ + b_{1,j} L_{j+2} \left(\frac{2z - a}{a} \right), \quad j = 1, \dots, N_z - 2,$$

$s \in \{x, y, z\}$, such that

$$\partial_z \Psi_{1,j}(a) - i\gamma^{(1)} \Psi_{1,j}(a) = 0, \quad \Psi_{1,j}(0) = 0,$$

where

$$\Psi_{1,j}(z) := (\psi_{1,j}^x, \psi_{1,j}^y, \psi_{1,j}^z)^T.$$

Similarly, for $z \in I_2$, we define

$$\begin{aligned} \psi_{2,j}^s(z) := (1+i)L_j\left(\frac{b-2z}{b}\right) + a_{2,j}L_{j+1}\left(\frac{b-2z}{b}\right) \\ + b_{2,j}L_{j+2}\left(\frac{b-2z}{b}\right), \quad j = 1, \dots, N_z - 2, \end{aligned}$$

$s \in \{x, y, z\}$, such that

$$\partial_z \Psi_{2,j}(b) + i\gamma^{(2)} \Psi_{2,j}(b) = 0, \quad \Psi_{2,j}(0) = 0,$$

where

$$\Psi_{2,j}(z) = (\psi_{2,j}^x, \psi_{2,j}^y, \psi_{2,j}^z)^T.$$

Note that these Legendre–Galerkin basis functions vanish at the transition layer at $z = 0$. For this reason, we introduce additional (enriched) basis functions which have the value $(1+i)$ at $z = 0$:

$$\eta^s(z) := \begin{cases} \eta_1^s(z) = c_1 z + (1+i), & 0 \leq z \leq a, \\ \eta_2^s(z) = c_2 z + (1+i), & b \leq z \leq 0, \end{cases}$$

$s \in \{x, y, z\}$, where

$$\partial_z \eta_1^s(a) - i\gamma^{(1)} \eta_1^s(a) = 0, \quad \partial_z \eta_2^s(b) + i\gamma^{(2)} \eta_2^s(b) = 0.$$

We readily find

$$c_1 = \frac{i\gamma^{(1)}}{(1+i) - i\gamma^{(1)}a}, \quad c_2 = \frac{-i\gamma^{(2)}}{(1+i) + i\gamma^{(2)}b}.$$

With these we construct the basis functions defined on $\{b < z < a\}$

$$\tilde{\psi}_j(z) = \begin{cases} \psi_{1,j}^x(z), & 0 < z < a, \\ 0, & b < z < 0, \end{cases} \quad j = 0, \dots, N_z - 2,$$

and

$$\tilde{\psi}_{N_z+j-1}(z) = \begin{cases} 0, & 0 < z < a, \\ \psi_{2,j}^x(z), & b < z < 0, \end{cases} \quad j = 0, \dots, N_z - 2,$$

and

$$\tilde{\psi}_{2N_z+j-2}(z) = \begin{cases} \psi_{1,j}^y(z), & 0 < z < a, \\ 0, & b < z < 0, \end{cases} \quad j = 0, \dots, N_z - 2,$$

and

$$\tilde{\psi}_{3N_z+j-3}(z) = \begin{cases} 0, & 0 < z < a, \\ \psi_{2,j}^y(z), & b < z < 0, \end{cases} \quad j = 0, \dots, N_z - 2,$$

and

$$\tilde{\psi}_{4N_z+j-4}(z) = \begin{cases} \psi_{1,j}^z(z), & 0 < z < a, \\ 0, & b < z < 0, \end{cases} \quad j = 0, \dots, N_z - 2,$$

and

$$\tilde{\psi}_{5N_z+j-5}(z) = \begin{cases} 0, & 0 < z < a, \\ \psi_{2,j}^z(z), & b < z < 0, \end{cases} \quad j = 0, \dots, N_z - 2,$$

and finally,

$$\tilde{\psi}_{6N_z-6} = \eta^x, \quad \tilde{\psi}_{6N_z-5} = \eta^y, \quad \tilde{\psi}_{6N_z-4} = \eta^z.$$

Setting $\bar{N} = 6N_z - 4$, we write our numerical approximation

$$u_{N_z}(z) := \sum_{j=0}^{\bar{N}} \hat{u}_j \tilde{\psi}_j(y),$$

and seek

$$\mathbf{u} = (\hat{u}_0, \hat{u}_1, \dots, \hat{u}_{\bar{N}})^T,$$

where we are given

$$\mathbf{f} = (\hat{f}_0, \dots, \hat{f}_{6N_z-7})^T, \quad \hat{f}_j := (\mathcal{I}_N f, \tilde{\psi}_j), \quad j = 0, \dots, \bar{N}.$$

209 Here, f stands for the right hand side \mathbf{R}_m in (13).

We define the matrices

$$(A_{m,s})_{lj} = (\partial_y^2 \tilde{\psi}_{(m-1+2(s-1))(N_z-1)+j}, \tilde{\psi}_{(m-1+2(s-1))(N_z-1)+l})_{I_m} \\ + (\gamma_{p,q}^{(m)})^2 (\tilde{\psi}_{(m-1+2(s-1))(N_z-1)+j}, \tilde{\psi}_{(m-1+2(s-1))(N_z-1)+l})_{I_m},$$

where $0 \leq l, j \leq N_z - 2$, $1 \leq m \leq 2$, and $1 \leq s \leq 3$. We set the column vectors

$$\begin{aligned} a_{12} &= (\partial_z^2 \tilde{\psi}_{6N_z-6}, \tilde{\psi}_j)_{I_1} + (\gamma_{p,q}^{(1)})^2 (\tilde{\psi}_{6N_z-6}, \tilde{\psi}_j)_{I_1}, \\ b_{12} &= (\partial_z^2 \tilde{\psi}_{6N_z-6}, \tilde{\psi}_{N_z+j-1})_{I_2} + (\gamma_{p,q}^{(2)})^2 (\tilde{\psi}_{6N_z-6}, \tilde{\psi}_{N_z+j-1})_{I_2}, \\ c_{13} &= (\partial_z^2 \tilde{\psi}_{6N_z-5}, \tilde{\psi}_{2N_z+j-2})_{I_1} + (\gamma_{p,q}^{(1)})^2 (\tilde{\psi}_{6N_z-5}, \tilde{\psi}_{2N_z+j-2})_{I_1}, \\ d_{13} &= (\partial_z^2 \tilde{\psi}_{6N_z-5}, \tilde{\psi}_{3N_z+j-3})_{I_2} + (\gamma_{p,q}^{(2)})^2 (\tilde{\psi}_{6N_z-5}, \tilde{\psi}_{3N_z+j-3})_{I_2}, \\ e_{14} &= (\partial_z^2 \tilde{\psi}_{6N_z-4}, \tilde{\psi}_{4N_z+j-4})_{I_1} + (\gamma_{p,q}^{(1)})^2 (\tilde{\psi}_{6N_z-4}, \tilde{\psi}_{4N_z+j-4})_{I_1}, \\ f_{14} &= (\partial_z^2 \tilde{\psi}_{6N_z-4}, \tilde{\psi}_{5N_z+j-5})_{I_2} + (\gamma_{p,q}^{(2)})^2 (\tilde{\psi}_{6N_z-4}, \tilde{\psi}_{5N_z+j-5})_{I_2}, \end{aligned}$$

and row vectors

$$\begin{aligned} a_{21} &= (\partial_z^2 \tilde{\psi}_j, \tilde{\psi}_{6N_z-6})_{I_1} + (\gamma_{p,q}^{(1)})^2 (\tilde{\psi}_j, \tilde{\psi}_{6N_z-6})_{I_1} + \partial_z \tilde{\psi}_j(0) \overline{\tilde{\psi}_{6N_z-6}}(0), \\ b_{21} &= (\partial_z^2 \tilde{\psi}_{N_z+j-1}, \tilde{\psi}_{6N_z-6})_{I_2} + (\gamma_{p,q}^{(2)})^2 (\tilde{\psi}_{N_z+j-1}, \tilde{\psi}_{6N_z-6})_{I_2} \\ &\quad - \tau \partial_z \tilde{\psi}_{N_z+j-1}(0) \overline{\tilde{\psi}_{6N_z-6}}(0), \\ c_{31} &= (\partial_z^2 \tilde{\psi}_{2N_z+j-2}, \tilde{\psi}_{6N_z-5})_{I_1} + (\gamma_{p,q}^{(1)})^2 (\tilde{\psi}_{2N_z+j-2}, \tilde{\psi}_{6N_z-5})_{I_1} \\ &\quad + \partial_z \tilde{\psi}_{2N_z+j-2}(0) \overline{\tilde{\psi}_{6N_z-5}}(0), \\ d_{31} &= (\partial_z^2 \tilde{\psi}_{3N_z+j-3}, \tilde{\psi}_{6N_z-5})_{I_2} + (\gamma_{p,q}^{(2)})^2 (\tilde{\psi}_{3N_z+j-3}, \tilde{\psi}_{6N_z-5})_{I_2} \\ &\quad - \tau \partial_z \tilde{\psi}_{3N_z+j-3}(0) \overline{\tilde{\psi}_{6N_z-5}}(0), \\ e_{41} &= (\partial_z^2 \tilde{\psi}_{4N_z+j-4}, \tilde{\psi}_{6N_z-4})_{I_1} + (\gamma_{p,q}^{(1)})^2 (\tilde{\psi}_{4N_z+j-4}, \tilde{\psi}_{6N_z-4})_{I_1} \\ &\quad + \partial_z \tilde{\psi}_{4N_z+j-4}(0) \overline{\tilde{\psi}_{6N_z-4}}(0), \\ f_{41} &= (\partial_z^2 \tilde{\psi}_{5N_z+j-5}, \tilde{\psi}_{6N_z-4})_{I_2} + (\gamma_{p,q}^{(2)})^2 (\tilde{\psi}_{5N_z+j-5}, \tilde{\psi}_{6N_z-4})_{I_2} \\ &\quad - \partial_z \tilde{\psi}_{5N_z+j-5}(0) \overline{\tilde{\psi}_{6N_z-4}}(0), \end{aligned}$$

for $0 \leq j \leq N_z - 2$. Moreover, we set

$$\begin{aligned}
a_{22} &= (\partial_z^2 \tilde{\psi}_{6N_z-6} + \kappa^2 \tilde{\psi}_{6N_z-6}, \tilde{\psi}_{6N_z-6}) \\
&\quad + \partial_z \tilde{\psi}_{6N_z-6}(0^+) \bar{\tilde{\psi}}_{6N_z-6}(0^+) - \tau \partial_z \tilde{\psi}_{6N_z-6}(0^-) \bar{\tilde{\psi}}_{6N_z-6}(0^-), \\
a_{33} &= (\partial_z^2 \tilde{\psi}_{6N_z-5} + \kappa^2 \tilde{\psi}_{6N_z-5}, \tilde{\psi}_{6N_z-5}) \\
&\quad + \partial_z \tilde{\psi}_{6N_z-5}(0^+) \bar{\tilde{\psi}}_{6N_z-5}(0^+) - \tau \partial_z \tilde{\psi}_{6N_z-5}(0^-) \bar{\tilde{\psi}}_{6N_z-5}(0^-), \\
a_{44} &= (\partial_z^2 \tilde{\psi}_{6N_z-4} + \kappa^2 \tilde{\psi}_{6N_z-4}, \tilde{\psi}_{6N_z-4}) \\
&\quad + \partial_z \tilde{\psi}_{6N_z-4}(0^+) \bar{\tilde{\psi}}_{6N_z-4}(0^+) - \partial_z \tilde{\psi}_{6N_z-4}(0^-) \bar{\tilde{\psi}}_{6N_z-4}(0^-), \\
a_{24} &= -i\alpha(1 - \tau) \tilde{\psi}_{6N_z-4}(0) \bar{\tilde{\psi}}_{6N_z-6}(0), \\
a_{34} &= -i\beta(1 - \tau) \tilde{\psi}_{6N_z-4}(0) \bar{\tilde{\psi}}_{6N_z-5}(0).
\end{aligned}$$

Here, $\partial_z \tilde{\psi}_n(0^-)$ and $\partial_z \tilde{\psi}_n(0^+)$ stand for the left and right derivatives at 0, respectively. The Legendre–Galerkin scheme demands the $6N_z - 3$ equations:

$$\mathbf{M}\mathbf{u} = \mathbf{f},$$

where \mathbf{M} is a block matrix

$$\mathbf{M} = \begin{pmatrix} A & B \\ C & D \end{pmatrix}.$$

The block matrix A is defined as

$$A = \begin{pmatrix} A_{1,1} & 0 & \dots & & 0 \\ 0 & A_{2,1} & & & \\ & & A_{1,2} & & \vdots \\ \vdots & & & A_{2,2} & \\ 0 & & \dots & & A_{1,3} & 0 \\ & & & & 0 & A_{2,3} \end{pmatrix},$$

and the block matrices B and C are defined as

$$B = \begin{pmatrix} a_{12} & 0 & 0 \\ b_{12} & 0 & \\ 0 & c_{13} & 0 \\ 0 & d_{13} & 0 \\ 0 & 0 & e_{14} \\ 0 & 0 & f_{14} \end{pmatrix},$$

and

$$C = \begin{pmatrix} (a_{21})^T & (b_{21})^T & 0 & 0 & 0 & 0 \\ 0 & 0 & (c_{31})^T & (d_{31})^T & 0 & 0 \\ 0 & 0 & 0 & 0 & (e_{41})^T & (f_{41})^T \end{pmatrix}.$$

Finally the upper-triangular matrix D is given by

$$D = \begin{pmatrix} a_{22} & 0 & a_{24} \\ 0 & a_{33} & a_{34} \\ 0 & 0 & a_{44} \end{pmatrix}.$$

210 6. Numerical Simulations

211 We now present a variety of numerical experiments utilizing our imple-
 212 mentation of the algorithm described above which demonstrate the stability,
 213 speed, and accuracy of our methodology. To begin, we demonstrate the per-
 214 formance of our solver for the boundary value problem (13) at the heart of
 215 our numerical method using an exact solution. Subsequently we display the
 216 fidelity of our *full* scattering solver for (10) using the “energy defect” as an
 217 indicator of convergence [Pet80].

218 6.1. Simulations of a Boundary Value Problem

We began by investigating our scheme’s numerical approximation of solutions to the reduced problem, (13), which is at the core of our full solver. Utilizing the algorithm proposed in Section 5, we looked for numerical convergence to solutions of the following one-dimensional reduced problem

$$\partial_z^2 \mathbf{u} + \mathbf{k}_u^2 \mathbf{u} = \mathbf{f}_u, \quad 0 < z < a, \quad (14a)$$

$$\partial_z^2 \mathbf{v} + \mathbf{k}_v^2 \mathbf{v} = \mathbf{f}_v, \quad b < z < 0, \quad (14b)$$

$$\mathbf{u}(0) = \mathbf{v}(0), \quad (14c)$$

$$\partial_z(u_1(0) - \tau v_1(0)) = i\alpha(u_3(0) - \tau v_3(0)), \quad (14d)$$

$$\partial_z(u_2(0) - \tau v_2(0)) = i\beta(u_3(0) - \tau v_3(0)), \quad (14e)$$

$$\partial_z(u_3(0) - v_3(0)) = 0, \quad (14f)$$

$$\partial_z \mathbf{u}(a) - i\gamma^{(1)} \mathbf{u}(a) = 0, \quad (14g)$$

$$\partial_z \mathbf{v}(b) + i\gamma^{(2)} \mathbf{v}(b) = 0, \quad (14h)$$

where

$$\begin{aligned}\mathbf{u} &= (u_1, u_2, u_3)^T, & \mathbf{v} &= (v_1, v_2, v_3)^T, \\ \mathbf{k}_u^2 &= ((k_{u1})^2, (k_{u2})^2, (k_{u3})^2)^T, & \mathbf{k}_v^2 &= ((k_{v1})^2, (k_{v2})^2, (k_{v3})^2)^T, \\ \mathbf{f}_u &= (f_{u1}, f_{u2}, f_{u3})^T, & \mathbf{f}_v &= (f_{v1}, f_{v2}, f_{v3})^T.\end{aligned}$$

219 Since the differential operator and boundary conditions in (14) are the same
220 as those in (13), the proposed model provides a good indicator of convergence
221 for our modified Legendre-Galerkin method.

As a test of convergence we considered the following functions and parameters

$$\begin{aligned}u_1 &= (y - a)^2(y + b)^2, & u_2 &= \sin(y)(y - a)^2(y + b)^2, \\ u_3 &= \exp(y)(y - a)^2(y + b)^2, \\ v_1 &= (y - a)^2(y + b)^2, & v_2 &= \sin(y)(y - a)^2(y + b)^2, \\ v_3 &= \exp(y)(y - a)^2(y + b)^2, \\ a &= 5, & b &= -2, & \tau &= 1.5, & \gamma^{(1)} &= 1 - i, & \gamma^{(2)} &= 2 + i, \\ (k_{u1}, k_{u2}, k_{u3}) &= (1.25, 2.25, 3.25), & (k_{v1}, k_{v2}, k_{v3}) &= (2.55, 3.55, 4.55).\end{aligned}\quad (15)$$

222 Upon using (14a) and (14b) we can define appropriate \mathbf{f}_u and \mathbf{f}_v so that these
223 represent an exact solution.

224 To test numerical convergence, we defined the relative L^2 error

$$\frac{\|u_{\text{ex}} - u_{N_z}\|_{L^2}}{\|u_{\text{ex}}\|_{L^2}}, \quad (16)$$

225 where u_{ex} is the exact solution and N_z is the number of Legendre-Galerkin
226 basis functions. In Figures 2 and 3 we display the spectral rate of con-
227 vergence which our Legendre-Galerkin method achieved in this simplified
228 setting. The numerical results illustrate that, given N_z chosen large enough,
229 the proposed modified spectral method can successfully resolve the vector
230 Helmholtz equations with the underlying interfacial boundary conditions.

231 *6.2. Simulations of a Layered Medium: The Maxwell Equations*

We also performed numerical experiments of a periodic doubly layered medium whose scattering returns are governed by the full vector Maxwell equations in three dimensions, (10). Unlike the simplified problem in Section 6.1, exact solutions are not available. Hence, we utilized the widely accepted

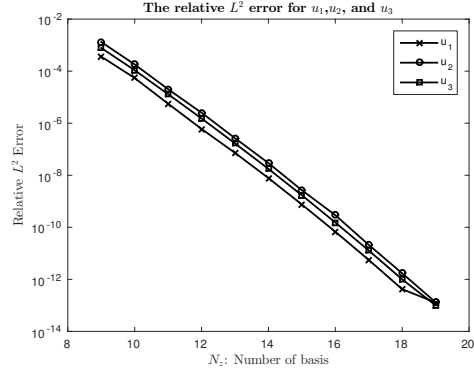


Figure 2: Relative L^2 error in \mathbf{u} , (16), of our Legendre–Galerkin approximation of (14) in configuration (15) versus number of basis functions N_z on a log–linear scale.

diagnostic of error measurement, the energy defect [Pet80, BR93a]. More precisely, if one considers the Rayleigh expansions in the upper and lower layers

$$\begin{aligned}\mathbf{H}_1(x, y, z) &= \sum_{p=-\infty}^{\infty} \sum_{q=-\infty}^{\infty} \hat{\mathbf{H}}_{1,p,q} e^{i(\alpha_p x + \beta_q y + \gamma^{(1)} z)}, \\ \mathbf{H}_2(x, y, z) &= \sum_{p=-\infty}^{\infty} \sum_{q=-\infty}^{\infty} \hat{\mathbf{H}}_{2,p,q} e^{i(\alpha_p x + \beta_q y - \gamma^{(2)} z)},\end{aligned}$$

quantities of great interest are the *efficiencies*

$$\begin{aligned}e_1^{p,q} &:= \frac{\gamma_{p,q}^{(1)}}{\gamma} \frac{|\hat{\mathbf{H}}_{1,p,q}|^2}{|\mathbf{A}|^2}, & (p, q) \in \mathcal{U}^1, \\ e_2^{p,q} &:= \frac{\gamma_{p,q}^{(2)}}{\gamma} \frac{|\hat{\mathbf{H}}_{2,p,q}|^2}{|\mathbf{A}|^2}, & (p, q) \in \mathcal{U}^2,\end{aligned}$$

where \mathbf{A} is the amplitude of the incident wave, (1). With this definition in hand, it is clear why these efficiencies are of such interest as they quantify the energy fraction in each mode which propagates away from the grating. If all materials in the structure are lossless ($k_m \in \mathbf{R}$), energy is conserved which is expressed as

$$\sum_{(p,q) \in \mathcal{U}^1} e_1^{p,q} + \tau \sum_{(p,q) \in \mathcal{U}^2} e_2^{p,q} = 1.$$

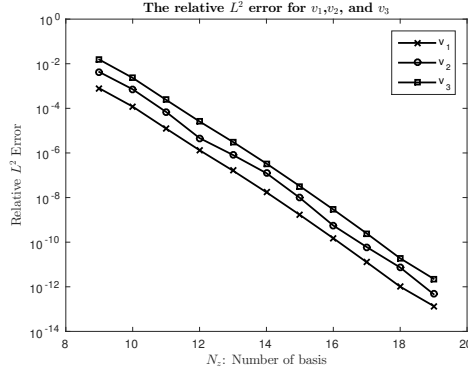


Figure 3: Relative L^2 error in \mathbf{v} , (16), of our Legendre–Galerkin approximation of (14) in configuration (15) versus number of basis functions N_z on a log–linear scale.

Hence, we define the “energy defect” as

$$\delta_d := 1 - \sum_{(p,q) \in \mathcal{U}^1} e_1^{p,q} - \tau \sum_{(p,q) \in \mathcal{U}^2} e_2^{p,q},$$

232 which will be zero for an exact solution [Pet80].

We conducted a sequence of simulations to show the spectral convergence of our proposed Legendre–Galerkin method (in the energy defect measure), and checked the performance of our numerical methods. To begin, we set the following configuration:

$$\begin{aligned} a &= 4, & b &= -3, & (\alpha, \beta, \gamma) &= (\sqrt{1/2}, \sqrt{1/3}, 1.2845), & d_1 &= d_2 = 2\pi, \\ \mathbf{A} &= (\sqrt{3}, \sqrt{3}, \sqrt{3}), & (\gamma^{(1)}, \gamma^{(2)}) &= (1.2845, 2.0330), \\ (k_1, k_2) &= (1.5758, 2.2285), & g(x, y) &= \varepsilon \cos(x) \cos(y). \end{aligned} \quad (17)$$

233 To characterize the performance of our methods we defined the parameters
 234 N (perturbation order) and $\{N_x, N_y, N_z\}$ (the number of basis functions in
 235 $\{x, y, z\}$ directions). In the first experiment we chose

$$N_x = N_y = 16, \quad N_z = 20, \quad (18)$$

236 and varied N . In Figure 4 we display the energy defect versus the number of
 237 perturbation orders, N , retained for the configuration (17) and the parameter
 238 choices (18). The figure shows the spectral convergence of the energy defect

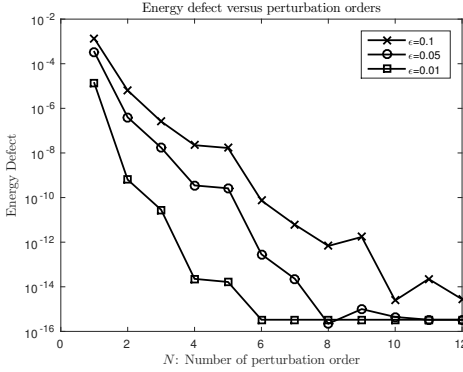


Figure 4: Energy defect versus perturbation order, N , for smooth interface configuration (17) and parameter choices (18).

as the perturbation order is refined. We also see that the energy defect decays more rapidly to machine precision as the value of ε is reduced.

In Figure 5 we display results of simulations of configuration (17) with parameter choices

$$N = 12, \quad N_x = N_y = 18, \quad (19)$$

while varying the vertical discretization parameter, N_z . This clearly shows the spectral convergence of the energy defect as this vertical discretization parameter is refined.

In Figures 6–9 we present the real parts of the scattered solution H^x and H^z from configuration (17) with parameter choices (18) where $\varepsilon = 0.05$. Figures 6 and 8 present the numerical approximations of H^x and H^z *above* the interface, $\{z = g(x, y)\}$, and Figures 7 and 9 display the numerical solutions of H^x and H^z *below* the interface, $\{z < g(x, y)\}$.

To continue, we investigate the possibility of using our new algorithm for deformations of *large* size. To examine this, we used the following configuration:

$$\begin{aligned} a &= 2, \quad b = -2, \quad (\alpha, \beta, \gamma) = (\sqrt{1/2}, \sqrt{1/3}, 1.2845), \quad d_1 = d_2 = 2\pi, \\ \mathbf{A} &= (\sqrt{3}, \sqrt{3}, \sqrt{3}), \quad (\gamma^{(1)}, \gamma^{(2)}) = (1.2845, 2.0330), \\ (k_1, k_2) &= (1.5758, 2.2285), \quad g(x, y) = \varepsilon \cos(x) \cos(y), \end{aligned} \quad (20)$$

with numerical parameters $(N_x, N_y, N_z) = (24, 24, 50)$. In Figure 10, we display numerical simulations with $\varepsilon = 1$. As exhibited in [NR01b, NR04a],

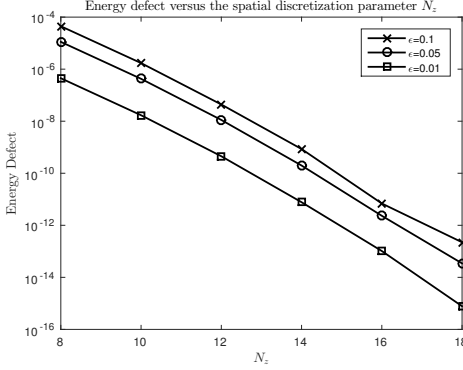


Figure 5: Energy defect versus perturbation order, N , for smooth interface configuration (17) and (18).

253 simple Taylor summation in perturbation order N does not work well for large
 254 or rough deformations. However, if Padé approximation [BGM96] is utilized
 255 then outstanding results can be achieved showing that *large* deformations
 256 can be readily simulated.

To close, we conducted a numerical simulation with a very *rough* interface defined with the aid of the following “sawtooth” profile

$$f_L(x) = \begin{cases} -\frac{2}{\pi}x + 1, & 0 \leq x \leq \pi, \\ \frac{2}{\pi}x - 3, & \pi \leq x \leq 2\pi, \end{cases}$$

where f_L possesses only Lipschitz regularity [NR04a, NR04b]. For our numerical experiments we used its Fourier series representation

$$f_L(x) = \sum_{k=1}^{\infty} \frac{8}{\pi^2(2k-1)^2} \cos((2k-1)x),$$

which we truncated after wavenumber $P = 20$,

$$f_{L,P}(x) = \sum_{k=1}^P \frac{8}{\pi^2(2k-1)^2} \cos((2k-1)x).$$

For these simulations we chose the following parameters:

$$\begin{aligned} a &= 2, & b &= -2, & (\alpha, \beta, \gamma) &= (0.2, 0.15, 0.35), & d_1 &= d_2 = 2\pi, \\ \mathbf{A} &= (\sqrt{3}, \sqrt{3}, \sqrt{3}), & (\gamma^{(1)}, \gamma^{(2)}) &= (0.35, 0.55453), \\ (k_1, k_2) &= (0.43012, 0.60828), & g(x, y) &= \varepsilon f_L(x) \cos(y), \end{aligned} \quad (21)$$

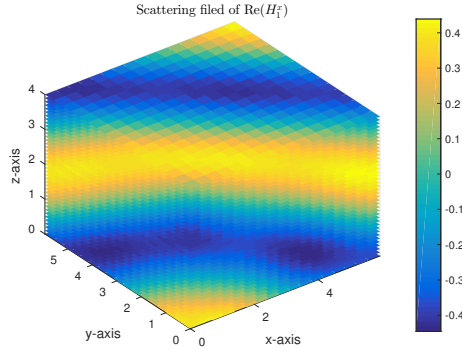


Figure 6: Plot of the real part of the scattered field $\text{Re}[H^x]$ above the interface in configuration (17) with parameters (18); for this we chose $\varepsilon = 0.05$ and $N = 12$.

257 with numerical parameters $(N_x, N_y, N_z) = (60, 18, 18)$. In Figure 11 we dis-
 258 play results of our experiment with this rough interface and $\varepsilon = 0.01, 0.05, 0.1$.
 259 Evidently, our new method is applicable to configurations with even Lipschitz
 260 smoothness, provided that sufficient resolution is utilized.

261 **7. Conclusions**

262 We have studied a HOPS algorithm for vector electromagnetic scattering
 263 by a periodic, doubly layered medium. In reformulating the time-harmonic
 264 Maxwell's equations, a system of vector Helmholtz equations was considered,
 265 together with appropriate interfacial boundary conditions. We introduced
 266 the TFE algorithm to the resulting problem for the first time, which required
 267 that we derive a sequence of one-dimensional, boundary value problems to be
 268 solved at each perturbation order in our expansion. Accurate numerical sim-
 269 lations of these TFE recursions were demonstrated with a Legendre-Galerkin
 270 method based on a novel weak formulation. These simulations included not
 271 only small and smooth interfaces in the periodic structure, but also large and
 272 rough ones as well. The numerical simulations showed the spectral conver-
 273 gence which our new algorithm can achieve, and our developments clearly
 274 point towards several extensions of great importance. In particular, our ap-
 275 proach will be generalized to accommodate surface currents which are one
 276 popular approach to modeling two-dimensional materials such as graphene
 277 and black phosphorous which are of such great interest to engineers at the

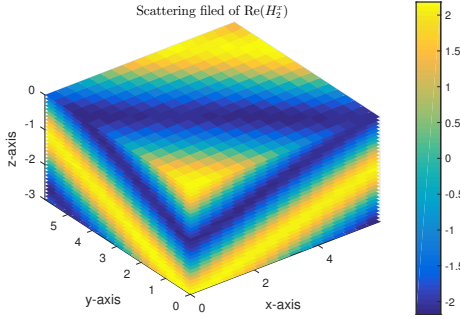


Figure 7: Plot of the real part of the scattered field $\text{Re}[H_z^x]$ below the interface in configuration (17) with parameters (18); for this we chose $\varepsilon = 0.05$ and $N = 12$.

278 moment [GN07, BFPV13]. This extension will not be straightforward as
 279 more subtle boundary conditions between layers must be considered, and
 280 hence the algorithmic differences will be significant. In addition, the natural
 281 extension to an arbitrary number of layers is clearly in view, and will be con-
 282 sidered in a forthcoming article. **For a potential roadmap we point the reader**
 283 **to [HN17a] where we achieved this in the simpler context of the Helmholtz**
 284 **equation.**

285 **Acknowledgements**

286 Y.H. gratefully acknowledges support from the Simons Foundation. D.P.N.
 287 gratefully acknowledges support from the National Science Foundation through
 288 grant No. DMS-1522548. The authors wish to thank Paul Martin and Peter
 289 Monk for their advice and guidance.

290 **Appendix A. Derivation of the Transformed Equations**

In this appendix we provide a full derivation of the transformed equations (11) presented in Section 3.1. Setting $g(x) = \varepsilon f(x)$, by the chain rule, we find

$$\begin{aligned}\partial_x &= \partial_{x'} + (\partial_x z_m) \partial_{z_m}, \quad m = 1, 2, \\ \partial_y &= \partial_{y'} + (\partial_y z_m) \partial_{z_m}, \quad m = 1, 2, \\ \partial_z &= (\partial_z z_m) \partial_{z_m}, \quad m = 1, 2.\end{aligned}$$

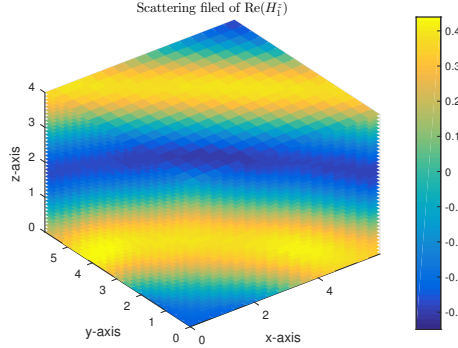


Figure 8: Plot of the real part of the scattered field $\text{Re}[H^z]$ above the interface in configuration (17) with parameters (18); for this we chose $\varepsilon = 0.05$ and $N = 12$.

With this we can write

$$\begin{aligned} (a - g)\nabla_{x,y} &= (a - g)\nabla_{x',y'} - (\nabla_{x',y'}g)(a - z_1)\partial_{z_1}, \\ (a - g)\partial_z &= a\partial_{z_1}, \end{aligned}$$

and

$$\begin{aligned} (b - g)\nabla_{x,y} &= (b - g)\nabla_{x',y'} - (\nabla_{x',y'}g)(z_2 - b)\partial_{z_2}, \\ (b - g)\partial_z &= b\partial_{z_2}, \end{aligned}$$

where $\nabla_{x,y} = (\partial_x, \partial_y)$ and $\nabla_{x',y'} = (\partial_{x'}, \partial_{y'})$. Defining

$$C_1 = (a - g), \quad D_1^x = -\partial_x g(a - z_1), \quad D_1^y = -\partial_y g(a - z_1), \quad G_1 = a,$$

and

$$C_2 = (b - g), \quad D_2^x = -\partial_x g(b - z_2), \quad D_2^y = -\partial_y g(b - z_2), \quad G_2 = -b,$$

we deduce that

$$\begin{aligned} C_m \partial_x &= C_m \partial_{x'} + D_m^x \partial_{z_m}, \\ C_m \partial_y &= C_m \partial_{y'} + D_m^y \partial_{z_m}, \\ C_m \partial_z &= G_m \partial_{z_m}, \end{aligned}$$

²⁹¹ for $m = 1, 2$.

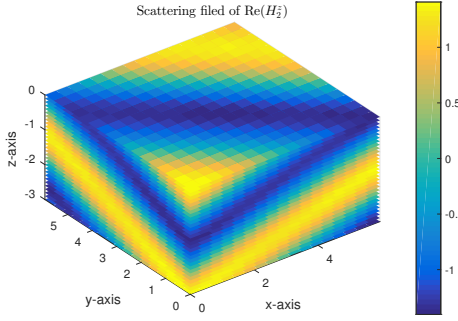


Figure 9: Plot of the real part of the scattered field $\text{Re}[H_z^s]$ below the interface in configuration (17) with parameters (18); for this we chose $\varepsilon = 0.05$ and $N = 12$.

292 *Appendix A.1. The Helmholtz Equation*

As in [HN17a], we rewrite the Laplace operator as

$$\begin{aligned} C_m^2 \Delta &= \nabla_{x',y'} \cdot [C_m^2 \nabla_{x',y'}] - (\nabla_{x',y'} C_m) \cdot [C_m \nabla_{x',y'}] + \partial_{z_m} [C_m D_m \cdot \nabla_{x',y'}] \\ &\quad - (\partial_{z_m} D_m) \cdot [C_m \nabla_{x',y'}] + \nabla_{x',y'} \cdot [C_m D_m \partial_{z_m}] - (\nabla_{x',y'} C_m) \cdot [D_m \partial_{z_m}] \\ &\quad + \partial_{z_m} [|D_m|^2 \partial_{z_m}] - (\partial_{z_m} D_m) \cdot [D_m \partial_{z_m}] - (\nabla_{x',y'} C_m) \cdot [C_m \nabla_{x',y'}] \\ &\quad - (\nabla_{x',y'} C_m) \cdot [D_m \partial_{z_m}] + G_m^2 \partial_{z_m}^2. \end{aligned}$$

where $D_m := (D_m^x, D_m^y)$. Then the governing problem becomes

$$\begin{aligned} 0 &= C_m^2 \Delta_m U_m + C_m^2 k_m^2 U_m \\ &= \nabla_{x',y'} \cdot (C_m^2 \nabla_{x',y'} U_m) + \partial_{z_m} (C_m D_m \cdot \nabla_{x',y'} U_m) + \nabla_{x',y'} \cdot (C_m D_m \partial_{z_m} U_m) \\ &\quad - (\nabla_{x',y'} C_m) \cdot (D_m \partial_{z_m} U_m) + \partial_{z_m} (|D_m|^2 \partial_{z_m} U_m) \\ &\quad - (\nabla_{x',y'} C_m) \cdot (C_m \nabla_{x',y'} U_m) + G_m^2 \partial_{z_m}^2 U_m + C_j^2 k_m^2 U_m, \end{aligned}$$

293 where U_m stands for the x , y , or z components of $\mathbf{U}_m = (U_m^x, U_m^y, U_m^z)^T$.
294 Setting $C_m^2(x) = G_m^2 + F_m(x)$ we deduce that

$$\Delta_m U_m + k_m^2 U_m = \frac{1}{G_m^2} (\partial_{x'} R_m^x + \partial_{y'} R_m^y + \partial_{z_m} R_m^z + R_m^0), \quad (\text{A.1})$$

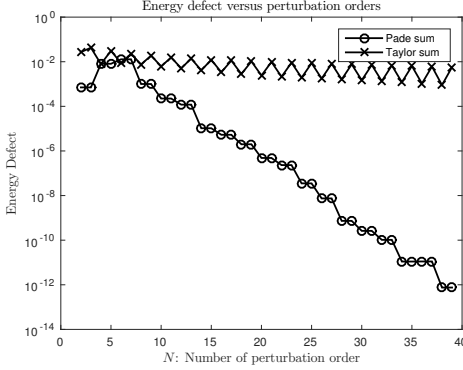


Figure 10: Energy defect versus perturbation order, N , for smooth interface configuration with large deformation (20).

where

$$R_m^x = -F_m \partial_{x'} U_m - C_m D_m^x \partial_{z_m} U_m, \quad (\text{A.2a})$$

$$R_m^y = -F_m \partial_{y'} U_m - C_m D_m^y \partial_{z_m} U_m, \quad (\text{A.2b})$$

$$\begin{aligned} R_m^z = & -C_m D_m^x \partial_{x'} U_m - (D_m^x)^2 \partial_{z_m} U_m \\ & - C_m D_m^y \partial_{y'} U_m - (D_m^y)^2 \partial_{z_m} U_m, \end{aligned} \quad (\text{A.2c})$$

$$\begin{aligned} R_m^0 = & (\partial_{x'} C_m) (D_m^x \partial_{z_m} U_m + C_m \partial_{x'} U_m) \\ & + (\partial_{y'} C_m) (D_m^y \partial_{z_m} U_m + C_m \partial_{y'} U_m) - F_m k_m^2 U_m. \end{aligned} \quad (\text{A.2d})$$

295 *Appendix A.2. Artificial Boundary Conditions*

For the conditions at the artificial boundaries, $\{z = a\}$ and $\{z = b\}$, of (10), we note that

$$\partial_{z_m} U_m - \frac{C_m}{G_m} T_m[U_m] = 0,$$

296 and obtain

$$\partial_{z_m} U_m - T_m[U_m] = -\frac{g}{M_m} T_m[U_m], \quad (\text{A.3})$$

297 for $M_1 = a$ and $M_2 = b$.

298 *Appendix A.3. Interfacial Boundary Conditions*

Regarding the transmission boundary conditions at $z = g(x, y)$ in (10),

$$\mathbf{N} \times (\mathbf{H}_1 - \mathbf{H}_2) = -\mathbf{N} \times \mathbf{H}^{inc},$$

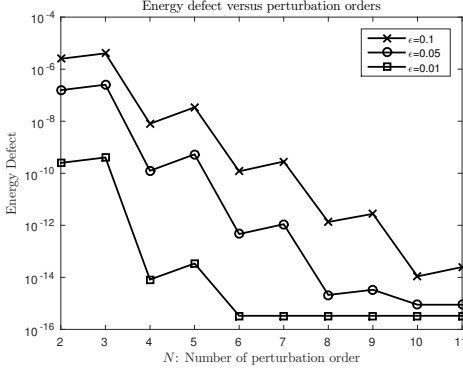


Figure 11: Energy defect versus perturbation order, N , for rough interface configuration (21).

implies that

$$\begin{aligned} (-\partial_{y'}g)\llbracket U^z \rrbracket - \llbracket U^y \rrbracket &= ((\partial_{y'}g)A^z + A^y)\varphi, \\ (-\partial_{x'}g)\llbracket U^z \rrbracket - \llbracket U^x \rrbracket &= ((\partial_{x'}g)A^z + A^x)\varphi. \end{aligned}$$

Furthermore

$$\mathbf{N} \times (\nabla \times (\mathbf{H}_1 - \tau \mathbf{H}_2)) = -\mathbf{N} \times (\nabla \times \mathbf{H}^{inc}),$$

implies that

$$\begin{aligned} (-\partial_y g)(\partial_x \llbracket H^y \rrbracket_\tau - \partial_y \llbracket H^x \rrbracket_\tau) + (\partial_x \llbracket H^z \rrbracket_\tau - \llbracket \partial_z H^x \rrbracket_\tau) \\ = (\partial_y g)(i\alpha A^y - i\beta A^x)\varphi - (i\alpha A^z + i\gamma A^x)\varphi, \quad (\text{A.4a}) \end{aligned}$$

and

$$\begin{aligned} (\partial_x g)(\partial_x \llbracket H^y \rrbracket_\tau - \partial_y \llbracket H^x \rrbracket_\tau) + (\partial_y \llbracket H^z \rrbracket_\tau - \llbracket \partial_z H^y \rrbracket_\tau) \\ = -(\partial_x g)(i\alpha A^y - i\beta A^x)\varphi - (i\alpha A^z + i\gamma A^y)\varphi. \quad (\text{A.4b}) \end{aligned}$$

Noting that, for any scalar function K ,

$$\begin{aligned}
\partial_x \llbracket K \rrbracket_\tau &= \partial_{x'}(K_1 - \tau K_2) + \left(\frac{D_1^x}{C_1} \partial_{z_1} K_1 - \tau \frac{D_2^x}{C_2} \partial_{z_2} K_2 \right) \\
&= \partial_{x'} \llbracket K \rrbracket_\tau + \left[\left[\frac{D^x}{C} \partial_z K \right] \right]_\tau, \\
\partial_y \llbracket K \rrbracket_\tau &= \partial_{y'}(K_1 - \tau K_2) + \left(\frac{D_1^y}{C_1} \partial_{z_1} K_1 - \tau \frac{D_2^y}{C_2} \partial_{z_2} K_2 \right) \\
&= \partial_{y'} \llbracket K \rrbracket_\tau + \left[\left[\frac{D^y}{C} \partial_z K \right] \right]_\tau, \\
\llbracket \partial_z K \rrbracket_\tau &= \frac{G_1}{C_1} \partial_{z_1} K_1 - \tau \frac{G_2}{C_2} \partial_{z_2} K_2 = \left[\left[\frac{G}{C} \partial_z K \right] \right]_\tau,
\end{aligned}$$

we rewrite (A.4) as

$$\begin{aligned}
&(-\partial_{y'} g) \left(\partial_{x'} \llbracket U^y \rrbracket_\tau + \left[\left[\frac{D^x}{C} \partial_z U^y \right] \right]_\tau - \partial_{y'} \llbracket U^x \rrbracket_\tau - \left[\left[\frac{D^y}{C} \partial_z U^x \right] \right]_\tau \right) \\
&+ \left(\partial_{x'} \llbracket U^z \rrbracket_\tau + \left[\left[\frac{D^x}{C} \partial_z U^z \right] \right]_\tau - \left[\left[\frac{G}{C} \partial_z U^x \right] \right]_\tau \right) \\
&= (\partial_{y'} g)(i\alpha A^y - i\beta A^x)\varphi - (i\alpha A^z + i\gamma A^x)\varphi, \tag{A.5}
\end{aligned}$$

and

$$\begin{aligned}
&(\partial_{x'} g) \left(\partial_{x'} \llbracket U^y \rrbracket_\tau + \left[\left[\frac{D^x}{C} \partial_z U^y \right] \right]_\tau - \partial_{y'} \llbracket U^x \rrbracket_\tau - \left[\left[\frac{D^y}{C} \partial_z U^x \right] \right]_\tau \right) \\
&+ \left(\partial_{y'} \llbracket U^z \rrbracket_\tau + \left[\left[\frac{D^y}{C} \partial_z U^z \right] \right]_\tau - \left[\left[\frac{G}{C} \partial_z U^y \right] \right]_\tau \right) \\
&= -(\partial_{x'} g)(i\alpha A^y - i\beta A^x)\varphi - (i\beta A^z + i\gamma A^y)\varphi. \tag{A.6}
\end{aligned}$$

Since $z_1 = z_2 = 0$ at $z = g(x, y)$, we have

$$D_1^x = (-\partial_{x'} g)a, \quad D_1^y = (-\partial_{y'} g)a, \quad D_2^x = (\partial_{x'} g)b, \quad D_2^y = (\partial_{y'} g)b.$$

Hence, we can simplify (A.5) and (A.6) as

$$\begin{aligned}
\partial_{x'} \llbracket U^z \rrbracket_\tau - \left[\left[\frac{G}{C} \partial_z U^x \right] \right]_\tau &= Q_1, \\
\partial_{y'} \llbracket U^z \rrbracket_\tau - \left[\left[\frac{G}{C} \partial_z U^y \right] \right]_\tau &= Q_2,
\end{aligned}$$

where

$$Q_1 := (\partial_{y'} g)(i\alpha A^y - i\beta A^x)\varphi - (i\alpha A^z + i\gamma A^x)\varphi - \left[\left[\frac{D^x}{C} \partial_z U^z \right] \right]_\tau \\ + (\partial_{y'} g) \left(\partial_{x'} \llbracket U^y \rrbracket_\tau + \left[\left[\frac{D^x}{C} \partial_z U^y \right] \right]_\tau - \partial_{y'} \llbracket U^x \rrbracket_\tau - \left[\left[\frac{D^y}{C} \partial_z U^x \right] \right]_\tau \right), \quad (\text{A.7a})$$

$$Q_2 := (-\partial_{x'} g)(i\alpha A^y - i\beta A^x)\varphi - (i\beta A^z + i\gamma A^y)\varphi - \left[\left[\frac{D^y}{C} \partial_z U^z \right] \right]_\tau \\ - (\partial_{x'} g) \left(\partial_{x'} \llbracket U^y \rrbracket_\tau + \left[\left[\frac{D^x}{C} \partial_z U^y \right] \right]_\tau - \partial_{y'} \llbracket U^x \rrbracket_\tau - \left[\left[\frac{D^y}{C} \partial_z U^x \right] \right]_\tau \right). \quad (\text{A.7b})$$

The divergence free boundary condition

$$C_m \partial_x H_m^x + C_m \partial_y H_m^y + C_m \partial_z H_m^z = 0,$$

transforms to

$$\partial_{x'} U_m^x + \partial_{y'} U_m^y + \frac{G_m}{C_m} \partial_{z_m} U_m^z = -\frac{D_m^x}{C_m} \partial_{z_m} U_m^x - \frac{D_m^y}{C_m} \partial_{z_m} U_m^y.$$

Hence, we deduce that

$$\partial_{x'} U_1^x + \partial_{y'} U_1^y + \frac{a}{a-g} \partial_{z_1} U_1^z = \frac{(\partial_{x'} g)a}{a-g} \partial_{z_1} U_1^x + \frac{(\partial_{y'} g)a}{a-g} \partial_{z_1} U_1^y, \\ \partial_{x'} U_2^x + \partial_{y'} U_2^y + \frac{b}{b-g} \partial_{z_2} U_2^z = \frac{(\partial_{x'} g)b}{b-g} \partial_{z_2} U_2^x + \frac{(\partial_{y'} g)b}{b-g} \partial_{z_2} U_2^y.$$

For the other interfacial boundary condition, we simply find that

$$\mathbf{N} \cdot \llbracket \mathbf{H} \rrbracket = -\mathbf{N} \cdot \mathbf{H}^{inc}$$

implies that

$$-\partial_{x'} g \llbracket U^x \rrbracket - \partial_{y'} g \llbracket U^y \rrbracket + \llbracket U^z \rrbracket = (\partial_{x'} g)\varphi + (\partial_{y'} g)\varphi - A^z \varphi.$$

Consequently, the transmission boundary conditions in (10) become

$$[\![U^x]\!] = (-\partial_{x'}g)[\![U^z]\!] + ((-\partial_{x'}g)A^z - A^x)\varphi, \quad (\text{A.8a})$$

$$[\![U^y]\!] = (-\partial_{y'}g)[\![U^z]\!] - ((\partial_{y'}g)A^z + A^y)\varphi, \quad (\text{A.8b})$$

$$[\![U^z]\!] = (\partial_{x'}g)[\![U^x]\!] + (\partial_{y'}g)[\![U^y]\!] + ((\partial_{x'}g)A^x + (\partial_{y'}g)A^y - A^z)\varphi, \quad (\text{A.8c})$$

$$\partial_{x'}[\![U^z]\!]_\tau - \left[\frac{G}{C} \partial_z U^x \right]_\tau = Q_1, \quad (\text{A.8d})$$

$$\partial_{y'}[\![U^z]\!]_\tau - \left[\frac{G}{C} \partial_z U^y \right]_\tau = Q_2, \quad (\text{A.8e})$$

$$\partial_{x'} U_1^x + \partial_{y'} U_1^y + \frac{a}{a-g} \partial_{z_1} U_1^z = \frac{(\partial_{x'}g)a}{a-g} \partial_{z_1} U_1^x + \frac{(\partial_{y'}g)a}{a-g} \partial_{z_1} U_1^y, \quad (\text{A.8f})$$

$$\partial_{x'} U_2^x + \partial_{y'} U_2^y + \frac{b}{b-g} \partial_{z_2} U_2^z = \frac{(\partial_{x'}g)b}{b-g} \partial_{z_2} U_2^x + \frac{(\partial_{y'}g)b}{b-g} \partial_{z_2} U_2^y. \quad (\text{A.8g})$$

²⁹⁹ *Appendix A.4. Boundary Perturbation*

Considering our specification that $g(x) = \varepsilon f(x)$, it can be shown that the following expansions converge strongly

$$U_m = \sum_{n=0}^{\infty} U_{m,n}(x, y, z) \varepsilon^n, \quad \text{for } m = 1, 2.$$

In light of this (A.1) becomes

$$\Delta_m U_{m,n} + k_m^2 U_{m,n} = \frac{1}{G_m^2} (\partial_{x'} R_{m,n}^x + \partial_{y'} R_{m,n}^y + \partial_{z_m} R_{m,n}^z + R_{m,n}^0) =: R_{m,n},$$

where

$$\begin{aligned} R_{m,n}^x &= (2M_m f) \partial_{x'} U_{m,n-1} + M_m \psi_m (\partial_{x'} f) \partial_{z_m} U_{m,n-1} \\ &\quad - f^2 \partial_{x'} U_{m,n-2} - f (\partial_{x'} f) \psi_m \partial_{z_m} U_{m,n-2}, \\ R_{m,n}^y &= (2M_m f) \partial_{y'} U_{m,n-1} + M_m \psi_m (\partial_{y'} f) \partial_{z_m} U_{m,n-1} \\ &\quad - f^2 \partial_{y'} U_{m,n-2} - f (\partial_{y'} f) \psi_m \partial_{z_m} U_{m,n-2}, \\ R_{m,n}^z &= M_m (\partial_{x'} f) \psi_m \partial_{x'} U_{m,n-1} + M_m (\partial_{y'} f) \psi_m \partial_{y'} U_{m,n-1} \\ &\quad - f (\partial_{x'} f) \psi_m \partial_{x'} U_{m,n-2} - f (\partial_{y'} f) \psi_m \partial_{y'} U_{m,n-2} \\ &\quad - \psi_m^2 ((\partial_{x'} f)^2 + (\partial_{y'} f)^2) \partial_{z_m} U_{m,n-2}, \\ R_{m,n}^0 &= -M_m (\partial_{x'} f) \partial_{x'} U_{m,n-1} - M_m (\partial_{y'} f) \partial_{y'} U_{m,n-1} \\ &\quad + 2M_m f k_m^2 U_{m,n-1} + ((\partial_{x'} f)^2 + (\partial_{y'} f)^2) \psi_m \partial_{z_m} U_{m,n-2} \\ &\quad + (\partial_{x'} f) f \partial_{x'} U_{m,n-2} + (\partial_{y'} f) f \partial_{y'} U_{m,n-2} - f^2 k_m^2 U_{m,n-2}. \end{aligned}$$

for

$$M_1 = a, \quad M_2 = b, \quad \psi_1 = a - z_1, \quad \psi_2 = b - z_2.$$

For the boundary condition (A.3), we write

$$\partial_{z_m} U_{m,n} - T_m[U_{m,n}] = -\frac{f}{M_m} T_m[U_{m,n-1}], \quad \text{for } m = 1, 2.$$

We now consider the transmission boundary conditions (A.8), and, upon setting

$$\varphi_n := e^{i(\alpha x' + \beta y')} \frac{(-i\gamma f)^n}{n!},$$

we write (A.8a) and (A.8b) as

$$\begin{aligned} \llbracket U_n^x \rrbracket &= (-\partial_{x'} f) \llbracket U_{n-1}^z \rrbracket - (\partial_{x'} f) A^z \varphi_{n-1} - A^x \varphi_n, \\ \llbracket U_n^y \rrbracket &= (-\partial_{y'} f) \llbracket U_{n-1}^z \rrbracket - (\partial_{y'} f) A^z \varphi_{n-1} - A^y \varphi_n, \end{aligned}$$

and (A.8c) as

$$\begin{aligned} \llbracket U_n^z \rrbracket &= (\partial_{x'} f) (U_{1,n-1}^x - U_{2,n-1}^x) + (\partial_{y'} f) (U_{1,n-1}^y - U_{2,n-1}^y) \\ &\quad + (\partial_{x'} f) A^x \varphi_{n-1} + (\partial_{y'} f) A^y \varphi_{n-1} - A^z \varphi_n. \end{aligned}$$

We reformulate (A.8d) and (A.8e) as

$$(\partial_{x'} U_{1,n}^z - \tau \partial_{x'} U_{2,n}^z) - \left(\frac{a}{a-g} \partial_{z_1} U_{1,n}^x - \tau \frac{b}{b-g} \partial_{z_2} U_{2,n}^x \right) = Q_{1,n}, \quad (\text{A.9a})$$

$$(\partial_{y'} U_{1,n}^z - \tau \partial_{y'} U_{2,n}^z) - \left(\frac{a}{a-g} \partial_{z_1} U_{1,n}^y - \tau \frac{b}{b-g} \partial_{z_2} U_{2,n}^y \right) = Q_{2,n}, \quad (\text{A.9b})$$

where

$$\begin{aligned} Q_{1,n} &= (\partial_{y'} f) (i\alpha A^y - i\beta A^x) \varphi_{n-1} - (i\alpha A^x + i\gamma A^x) \varphi_n \\ &\quad + \left(\frac{a \partial_{x'} f}{a-g} \partial_{z_1} U_{1,n-1}^z + \tau \frac{b \partial_{x'} f}{g-b} \partial_{z_2} U_{2,n-1}^z \right) \\ &\quad + (\partial_{y'} f) \left(\frac{(-\partial_{x'} f) a}{a-g} \partial_{z_1} U_{1,n-2}^y - \tau \frac{(\partial_{x'} f) b}{g-b} \partial_{z_2} U_{2,n-2}^y \right. \\ &\quad \left. - \frac{(-\partial_{y'} f) a}{a-g} \partial_{z_1} U_{1,n-2}^x + \tau \frac{(\partial_{y'} f) b}{g-b} \partial_{z_2} U_{2,n-2}^x \right) \\ &\quad + (\partial_{y'} f) (\partial_{x'} U_{1,n-1}^y - \tau \partial_{x'} U_{2,n-1}^y - \partial_{y'} U_{1,n-1}^x + \tau \partial_{y'} U_{2,n-1}^x), \end{aligned}$$

and

$$\begin{aligned}
Q_{2,n} = & (-\partial_{x'} f)(i\alpha A^y - i\beta A^x)\varphi_{n-1} - (i\beta A^z + i\gamma A^y)\varphi_n \\
& - \left(\frac{(-\partial_{y'} f)a}{a-g} \partial_{z_1} U_{1,n-1}^z - \tau \frac{(\partial_{y'} f)b}{g-b} \partial_{z_2} U_{2,n-1}^z \right) \\
& - (\partial_{x'} f) \left(\frac{(-\partial_{x'} f)a}{a-g} \partial_{z_1} U_{1,n-2}^y - \tau \frac{(\partial_{x'} f)b}{g-b} \partial_{z_2} U_{2,n-2}^y \right. \\
& \left. - \frac{(-\partial_{y'} f)a}{a-g} \partial_{z_1} U_{1,n-2}^x + \tau \frac{(\partial_{y'} f)b}{g-b} \partial_{z_2} U_{2,n-2}^x \right) \\
& - (\partial_{x'} f) (\partial_{x'} U_{1,n-1}^y - \tau \partial_{x'} U_{2,n-1}^y - \partial_{y'} U_{1,n-1}^x + \tau \partial_{y'} U_{2,n-1}^x).
\end{aligned}$$

Multiplying (A.9) by $(a-g)(b-g)$ we rearrange these equations

$$\begin{aligned}
(\partial_{x'} U_{1,n}^z - \tau \partial_{x'} U_{2,n}^z) - (\partial_{z_1} U_{1,n}^x - \tau \partial_{z_2} U_{2,n}^x) &= \tilde{Q}_{1,n}, \\
(\partial_{y'} U_{1,n}^z - \tau \partial_{y'} U_{2,n}^z) - (\partial_{z_1} U_{1,n}^y - \tau \partial_{z_2} U_{2,n}^y) &= \tilde{Q}_{2,n},
\end{aligned}$$

where

$$\begin{aligned}
\tilde{Q}_{1,n} = & \frac{1}{ab} (f(a+b)(\partial_{x'} U_{1,n-1}^z - \tau \partial_{x'} U_{2,n-1}^z) - af \partial_{z_1} U_{1,n-1}^x + \tau bf \partial_{z_2} U_{2,n-1}^x \\
& - f^2 \partial_{x'} U_{1,n-2}^z + \tau f^2 \partial_{x'} U_{2,n-2}^z + ab Q_{1,n} - (a+b)f Q_{1,n-1} + f^2 Q_{1,n-2}),
\end{aligned}$$

and

$$\begin{aligned}
\tilde{Q}_{2,n} = & \frac{1}{ab} (f(a+b)(\partial_{y'} U_{1,n-1}^z - \tau \partial_{y'} U_{2,n-1}^z) - af \partial_{z_1} U_{1,n-1}^y + \tau bf \partial_{z_2} U_{2,n-1}^y \\
& - f^2 \partial_{y'} U_{1,n-2}^z + \tau f^2 \partial_{y'} U_{2,n-2}^z + ab Q_{2,n} - (a+b)f Q_{2,n-1} + f^2 Q_{2,n-2}).
\end{aligned}$$

If we multiply (A.8f) by $(a-g)/a$ and (A.8g) by $(b-g)/b$, respectively, and simplify the divergence free conditions we find

$$\begin{aligned}
& \partial_{x'} U_{1,n}^x + \partial_{y'} U_{1,n}^y + \partial_{z_1} U_{1,n}^z \\
& = (\partial_{x'} f) \partial_{z_1} U_{1,n-1}^x + (\partial_{y'} f) \partial_{z_1} U_{1,n-1}^y + \frac{f}{a} \partial_{x'} U_{1,n-1}^x + \frac{f}{a} \partial_{y'} U_{1,n-1}^y,
\end{aligned}$$

and

$$\begin{aligned}
& \partial_{x'} U_{2,n}^x + \partial_{y'} U_{2,n}^y + \partial_{z_2} U_{2,n}^z \\
& = (\partial_{x'} f) \partial_{z_2} U_{2,n-1}^x + (\partial_{y'} f) \partial_{z_2} U_{2,n-1}^y + \frac{f}{b} \partial_{x'} U_{2,n-1}^x + \frac{f}{b} \partial_{y'} U_{2,n-1}^y.
\end{aligned}$$

By subtracting these equations, we complete the interfacial boundary condition

$$\partial_{x'}(U_{1,n}^x - U_{2,n}^x) + \partial_{y'}(U_{1,n}^y - U_{2,n}^y) + (\partial_{z_1}U_{1,n}^z - \partial_{z_2}U_{2,n}^z) = \tilde{J}_n,$$

where

$$\begin{aligned} \tilde{J}_n := & (\partial_{x'}f)(\partial_{z_1}U_{1,n-1}^x - \partial_{z_2}U_{2,n-1}^x) + (\partial_{y'}f)(\partial_{z_1}U_{1,n-1}^y - \partial_{z_2}U_{2,n-1}^y) \\ & + \left(\frac{f}{a}\partial_{x'}U_{1,n-1}^x - \frac{f}{b}\partial_{x'}U_{2,n-1}^x \right) + \left(\frac{f}{a}\partial_{y'}U_{1,n-1}^y - \frac{f}{b}\partial_{y'}U_{2,n-1}^y \right). \end{aligned}$$

In conclusion, we arrive at the following equations:

$$\Delta_1 \mathbf{U}_{1,n} + k_1^2 \mathbf{U}_{1,n} = \mathbf{R}_{1,n}, \quad \text{in } 0 < z < a, \quad (\text{A.10a})$$

$$\Delta_2 \mathbf{U}_{2,n} + k_2^2 \mathbf{U}_{2,n} = \mathbf{R}_{2,n}, \quad \text{in } b < z < 0, \quad (\text{A.10b})$$

$$[\![U_n^x]\!] = I_{1,n}, \quad \text{at } z_1 = z_2 = 0, \quad (\text{A.10c})$$

$$[\![U_n^y]\!] = I_{2,n}, \quad \text{at } z_1 = z_2 = 0, \quad (\text{A.10d})$$

$$[\![U_n^z]\!] = I_{3,n}, \quad \text{at } z_1 = z_2 = 0, \quad (\text{A.10e})$$

$$[\![\partial_{x'}U_n^z]\!]_\tau [\![\partial_zU_n^x]\!]_\tau = \tilde{Q}_1, \quad \text{at } z_1 = z_2 = 0, \quad (\text{A.10f})$$

$$[\![\partial_{y'}U_n^z]\!]_\tau [\![\partial_zU_n^y]\!]_\tau = \tilde{Q}_2, \quad \text{at } z_1 = z_2 = 0, \quad (\text{A.10g})$$

$$[\![\partial_{x'}U_n^x]\!] + [\![\partial_{y'}U_n^y]\!] + [\![\partial_zU_n^z]\!] = \tilde{J}_n, \quad \text{at } z_1 = z_2 = 0, \quad (\text{A.10h})$$

$$\partial_{z_1} \mathbf{U}_{1,n} - T_1[\mathbf{U}_{1,n}] = \mathbf{B}_{1,n}, \quad \text{at } z_1 = a, \quad (\text{A.10i})$$

$$\partial_{z_2} \mathbf{U}_{2,n} - T_2[\mathbf{U}_{2,n}] = \mathbf{B}_{2,n}, \quad \text{at } z_2 = b, \quad (\text{A.10j})$$

where

$$I_{1,n} := (-\partial_{x'}f)(U_{1,n-1}^z - U_{2,n-1}^z) - (\partial_{x'}f)A^z\varphi_{n-1} - A^x\varphi_n,$$

$$I_{2,n} := (-\partial_{y'}f)(U_{1,n-1}^z - U_{2,n-1}^z) - (\partial_{y'}f)A^z\varphi_{n-1} - A^y\varphi_n,$$

$$\begin{aligned} I_{3,n} := & (\partial_{x'}f)(U_{1,n-1}^x - U_{2,n-1}^x) + (\partial_{y'}f)(U_{1,n-1}^y - U_{2,n-1}^y) \\ & + (\partial_{x'}f)A^x\varphi_{n-1} + (\partial_{y'}f)A^y\varphi_{n-1} - A^z\varphi_n \end{aligned}$$

and

$$\mathbf{B}_{1,n} = -\frac{f}{a}T_1[\mathbf{U}_{1,n-1}],$$

$$\mathbf{B}_{2,n} = -\frac{f}{b}T_2[\mathbf{U}_{2,n-1}].$$

300 **References**

301 [AP10] H. A. Atwater and A. Polman. Plasmonics for improved photo-
302 voltaic devices. *Nat. Mater.*, 9:205, 2010.

303 [Are09] Tilo Arens. *Scattering by Biperiodic Layered Media: The Integral*
304 *Equation Approach*. Habilitationsschrift, Karlsruhe Institute of
305 Technology, 2009.

306 [BD14] O. Bruno and B. Delourme. Rapidly convergent two-
307 dimensional quasi-periodic Green function throughout the
308 spectrum—including Wood anomalies. *Journal of Computational*
309 *Physics*, 262:262–290, 2014.

310 [Bér94] Jean-Pierre Bérenger. A perfectly matched layer for the absorp-
311 tion of electromagnetic waves. *J. Comput. Phys.*, 114(2):185–
312 200, 1994.

313 [Bér99] Jean-Pierre Bérenger. Evanescent waves in PML’s: origin
314 of the numerical reflection in wave-structure interaction prob-
315 lems. *IEEE Trans. Antennas and Propagation*, 47(10):1497–
316 1503, 1999.

317 [BF95] Gang Bao and Avner Friedman. Inverse problems for scattering
318 by periodic structures. *Arch. Rational Mech. Anal.*, 132(1):49–
319 72, 1995.

320 [BFL17] Oscar P. Bruno and Agustin G. Fernandez-Lado. Rapidly
321 convergent quasi-periodic Green functions for scattering by
322 arrays of cylinders—including Wood anomalies. *Proc. A.*,
323 473(2199):20160802, 23, 2017.

324 [BFPV13] Y. Bludov, A. Ferreira, N. Peres, and M. Vasilevskiy. A primer on
325 surface plasmon-polaritons in graphene. *International Journal*
326 *of Modern Physics B*, 27:1341001, 2013.

327 [BG11] A. Barnett and L. Greengard. A new integral representation
328 for quasi-periodic scattering problems in two dimensions. *BIT*
329 *Numerical Mathematics*, 51:67–90, 2011.

330 [BGM96] George A. Baker, Jr. and Peter Graves-Morris. *Padé approxi-*
 331 *mants*. Cambridge University Press, Cambridge, second edition,
 332 1996.

333 [BLPAT16] Oscar P. Bruno, Mark Lyon, Carlos Pérez-Arcibia, and
 334 Catalin Turc. Windowed Green function method for layered-
 335 media scattering. *SIAM J. Appl. Math.*, 76(5):1871–1898, 2016.

336 [BNNW09] T. Binford, D. P. Nicholls, N. Nigam, and T. Warburton. Exact
 337 non-reflecting boundary conditions on general domains and hp-
 338 finite elements. *Journal of Scientific Computing*, 39(2):265–292,
 339 2009.

340 [BPA17] O. P. Bruno and C. Pérez-Arcibia. Windowed Green function
 341 method for the Helmholtz equation in the presence of multiply
 342 layered media. *Proc. A.*, 473(2202):20170161, 20, 2017.

343 [BR93a] O. Bruno and F. Reitich. Numerical solution of diffraction prob-
 344 lems: A method of variation of boundaries. *J. Opt. Soc. Am. A*,
 345 10(6):1168–1175, 1993.

346 [BR93b] O. Bruno and F. Reitich. Numerical solution of diffraction prob-
 347 lems: A method of variation of boundaries. II. Finitely conduct-
 348 ing gratings, Padé approximants, and singularities. *J. Opt. Soc.*
 349 *Am. A*, 10(11):2307–2316, 1993.

350 [BR93c] O. Bruno and F. Reitich. Numerical solution of diffraction prob-
 351 lems: A method of variation of boundaries. III. Doubly periodic
 352 gratings. *J. Opt. Soc. Am. A*, 10(12):2551–2562, 1993.

353 [BR94] Oscar P. Bruno and Fernando Reitich. Approximation of an-
 354 alytic functions: A method of enhanced convergence. *Math.*
 355 *Comp.*, 63(207):195–213, 1994.

356 [BR96] Oscar P. Bruno and Fernando Reitich. Calculation of electro-
 357 magnetic scattering via boundary variations and analytic continua-
 358 tion. *Appl. Comput. Electromagn. Soc. J.*, 11(1):17–31, 1996.

359 [BR98] Oscar P. Bruno and Fernando Reitich. Boundary-variation solu-
 360 tions for bounded-obstacle scattering problems in three dimen-
 361 sions. *J. Acoust. Soc. Am.*, 104(5):2579–2583, 1998.

362 [BR01] Oscar P. Bruno and Fernando Reitich. High-order boundary
 363 perturbation methods. In *Mathematical Modeling in Optical Sci-
 364 ence*, volume 22, pages 71–109. SIAM, Philadelphia, PA, 2001.
 365 Frontiers in Applied Mathematics Series.

366 [BSTV16] Oscar P. Bruno, Stephen P. Shipman, Catalin Turc, and
 367 Stephanos Venakides. Superalgebraically convergent smoothly
 368 windowed lattice sums for doubly periodic Green functions in
 369 three-dimensional space. *Proc. A.*, 472(2191):20160255, 19, 2016.

370 [CB15] Min Hyun Cho and Alex Barnett. Robust fast direct integral
 371 equation solver for quasi-periodic scattering problems with a
 372 large number of layers. *Optics Express*, 23(2):1775–1799, 2015.

373 [CF91] Xinfu Chen and Avner Friedman. Maxwell’s equations in a peri-
 374 odic structure. *Trans. Amer. Math. Soc.*, 323(2):465–507, 1991.

375 [CK13] David Colton and Rainer Kress. *Inverse acoustic and electro-
 376 magnetic scattering theory*, volume 93 of *Applied Mathematical
 377 Sciences*. Springer, New York, third edition, 2013.

378 [CMR80] J. Chandezon, D. Maystre, and G. Raoult. A new theoretical
 379 method for diffraction gratings and its numerical application. *J.
 380 Opt.*, 11(7):235–241, 1980.

381 [DF92] David Dobson and Avner Friedman. The time-harmonic
 382 Maxwell equations in a doubly periodic structure. *J. Math. Anal.
 383 Appl.*, 166(2):507–528, 1992.

384 [DFM02] M. O. Deville, P. F. Fischer, and E. H. Mund. *High-order meth-
 385 ods for incompressible fluid flow*, volume 9 of *Cambridge Mono-
 386 graphs on Applied and Computational Mathematics*. Cambridge
 387 University Press, Cambridge, 2002.

388 [ELG⁺98] T. W. Ebbesen, H. J. Lezec, H. F. Ghaemi, T. Thio, and
 389 P. A. Wolff. Extraordinary optical transmission through sub-
 390 wavelength hole arrays. *Nature*, 391(6668):667–669, 1998.

391 [FNS07] Q. Fang, D. P. Nicholls, and J. Shen. A stable, high-order
 392 method for three-dimensional bounded-obstacle scattering. *J.
 393 Comput. Phys.*, 224(2):1145–1169, 2007.

394 [Giv99] D. Givoli. Recent advances in the DtN FE method. *Arch. Comput. Methods Engrg.*, 6(2):71–116, 1999.

395

396 [GN07] A. Geim and K. Novoselov. The rise of graphene. *Nature Materials*, 6:183–191, 2007.

397

398 [GO77] D. Gottlieb and S. A. Orszag. *Numerical analysis of spectral*
399 *methods: theory and applications*. Society for Industrial and
400 Applied Mathematics, Philadelphia, Pa., 1977. CBMS-NSF Regional Conference Series in Applied Mathematics, No. 26.

401

402 [GR87] L. Greengard and V. Rokhlin. A fast algorithm for particle sim-
403 ulations. *J. Comput. Phys.*, 73(2):325–348, 1987.

404 [HN10] B. Hu and D. P. Nicholls. The domain of analyticity of Dirichlet–
405 Neumann operators. *Proceedings of the Royal Society of Edin-
406 burgh A*, 140(2):367–389, 2010.

407 [HN17a] Y. Hong and D. P. Nicholls. A high-order perturbation of sur-
408 faces method for scattering of linear waves by periodic multiply
409 layered gratings in two and three dimensions. *Journal of Com-
410 putational Physics*, 345:162–188, 2017.

411 [HN17b] Y. Hong and D. P. Nicholls. A stable high-order perturbation
412 of surfaces method for numerical simulation of diffraction prob-
413 lems in triply layered media. *Journal of Computational Physics*,
414 330:1043–1068, 2017.

415 [HNS12] Y. He, D. P. Nicholls, and J. Shen. An efficient and stable spec-
416 tral method for electromagnetic scattering from a layered peri-
417 odic structure. *Journal of Computational Physics*, 231(8):3007–
418 3022, 2012.

419 [Hom08] J. Homola. Surface plasmon resonance sensors for detection of
420 chemical and biological species. *Chemical Reviews*, 108(2):462–
421 493, 2008.

422 [HW85] Hou De Han and Xiao Nan Wu. Approximation of infinite
423 boundary condition and its application to finite element meth-
424 ods. *J. Comput. Math.*, 3(2):179–192, 1985.

425 [HW08] Jan S. Hesthaven and Tim Warburton. *Nodal discontinuous*
 426 *Galerkin methods*, volume 54 of *Texts in Applied Mathematics*.
 427 Springer, New York, 2008. Algorithms, analysis, and applica-
 428 tions.

429 [JN80] Claes Johnson and J.-Claude Nédélec. On the coupling of
 430 boundary integral and finite element methods. *Math. Comp.*,
 431 35(152):1063–1079, 1980.

432 [Joh87] Claes Johnson. *Numerical solution of partial differential equa-
 433 tions by the finite element method*. Cambridge University Press,
 434 Cambridge, 1987.

435 [JWP96] Bo-Nan Jiang, Jie Wu, and L. A. Povinelli. The origin of spurious
 436 solutions in computational electromagnetics. *J. Comput. Phys.*,
 437 125(1):104–123, 1996.

438 [KG89] Joseph B. Keller and Dan Givoli. Exact nonreflecting boundary
 439 conditions. *J. Comput. Phys.*, 82(1):172–192, 1989.

440 [KN99] Urve Kangro and Roy Nicolaides. Divergence boundary condi-
 441 tions for vector Helmholtz equations with divergence constraints.
 442 *M2AN Math. Model. Numer. Anal.*, 33(3):479–492, 1999.

443 [LeV07] Randall J. LeVeque. *Finite difference methods for ordinary and*
 444 *partial differential equations*. Society for Industrial and Applied
 445 Mathematics (SIAM), Philadelphia, PA, 2007. Steady-state and
 446 time-dependent problems.

447 [LJJ⁺12] N. C. Lindquist, T. W. Johnson, J. Jose, L. M. Otto, and S.-
 448 H. Oh. Ultrasmooth metallic films with buried nanostructures
 449 for backside reflection-mode plasmonic biosensing. *Annalen der*
 450 *Physik*, 524:687–696, 2012.

451 [Mil91a] D. Michael Milder. An improved formalism for rough-surface
 452 scattering of acoustic and electromagnetic waves. In *Proceedings*
 453 *of SPIE - The International Society for Optical Engineering (San*
 454 *Diego, 1991)*, volume 1558, pages 213–221. Int. Soc. for Optical
 455 Engineering, Bellingham, WA, 1991.

456 [Mil91b] D. Michael Milder. An improved formalism for wave scattering
 457 from rough surfaces. *J. Acoust. Soc. Am.*, 89(2):529–541, 1991.

458 [Mos85] M. Moskovits. Surface-enhanced spectroscopy. *Reviews of Mod-
 459 ern Physics*, 57(3):783–826, 1985.

460 [MS91] D. Michael Milder and H. Thomas Sharp. Efficient computation
 461 of rough surface scattering. In *Mathematical and numerical as-
 462 pects of wave propagation phenomena (Strasbourg, 1991)*, pages
 463 314–322. SIAM, Philadelphia, PA, 1991.

464 [MS92] D. Michael Milder and H. Thomas Sharp. An improved formal-
 465 ism for rough surface scattering. ii: Numerical trials in three
 466 dimensions. *J. Acoust. Soc. Am.*, 91(5):2620–2626, 1992.

467 [Nic15] D. P. Nicholls. A method of field expansions for vector electro-
 468 magnetic scattering by layered periodic crossed gratings. *Journal
 469 of the Optical Society of America, A*, 32(5):701–709, 2015.

470 [NN04] D. P. Nicholls and N. Nigam. Exact non-reflecting boundary
 471 conditions on general domains. *J. Comput. Phys.*, 194(1):278–
 472 303, 2004.

473 [NOJR16] D. P. Nicholls, S.-H. Oh, T. W. Johnson, and F. Reitich. Launch-
 474 ing surface plasmon waves via vanishingly small periodic grat-
 475 ings. *Journal of Optical Society of America, A*, 33(3):276–285,
 476 2016.

477 [NR01a] D. P. Nicholls and F. Reitich. A new approach to analyticity of
 478 Dirichlet-Neumann operators. *Proc. Roy. Soc. Edinburgh Sect.
 479 A*, 131(6):1411–1433, 2001.

480 [NR01b] D. P. Nicholls and F. Reitich. Stability of high-order perturbative
 481 methods for the computation of Dirichlet-Neumann operators. *J.
 482 Comput. Phys.*, 170(1):276–298, 2001.

483 [NR03] D. P. Nicholls and F. Reitich. Analytic continuation of Dirichlet-
 484 Neumann operators. *Numer. Math.*, 94(1):107–146, 2003.

485 [NR04a] D. P. Nicholls and F. Reitich. Shape deformations in rough
 486 surface scattering: Cancellations, conditioning, and convergence.
 487 *J. Opt. Soc. Am. A*, 21(4):590–605, 2004.

488 [NR04b] D. P. Nicholls and F. Reitich. Shape deformations in rough
 489 surface scattering: Improved algorithms. *J. Opt. Soc. Am. A*,
 490 21(4):606–621, 2004.

491 [NRJO14] D. P. Nicholls, F. Reitich, T. W. Johnson, and S.-H. Oh. Fast
 492 high-order perturbation of surfaces (HOPS) methods for simula-
 493 tion of multi-layer plasmonic devices and metamaterials. *Journal*
 494 *of the Optical Society of America, A*, 31(8):1820–1831, 2014.

495 [NS06] D. P. Nicholls and J. Shen. A stable, high-order method for two-
 496 dimensional bounded-obstacle scattering. *SIAM J. Sci. Com-
 497 put.*, 28(4):1398–1419, 2006.

498 [NS09] D. P. Nicholls and J. Shen. A rigorous numerical analysis of the
 499 transformed field expansion method. *SIAM Journal on Numer-
 500 ical Analysis*, 47(4):2708–2734, 2009.

501 [NT16] D. P. Nicholls and V. Tammali. A high-order perturbation of
 502 surfaces (HOPS) approach to Fokas integral equations: Vector
 503 electromagnetic scattering by periodic crossed gratings. *Applied
 504 Numerical Methods*, 101:1–17, 2016.

505 [Pet80] R. Petit, editor. *Electromagnetic theory of gratings*. Springer-
 506 Verlag, Berlin, 1980.

507 [Phi57] N. A. Phillips. A coordinate system having some special ad-
 508 vantages for numerical forecasting. *Journal of the Atmospheric
 509 Sciences*, 14(2):184–185, 1957.

510 [Ray07] Lord Rayleigh. On the dynamical theory of gratings. *Proc. Roy.
 511 Soc. London*, A79:399–416, 1907.

512 [Ric51] S. O. Rice. Reflection of electromagnetic waves from slightly
 513 rough surfaces. *Comm. Pure Appl. Math.*, 4:351–378, 1951.

514 [RT04] F. Reitich and K. Tamma. State-of-the-art, trends, and direc-
 515 tions in computational electromagnetics. *CMES Comput. Model.
 516 Eng. Sci.*, 5(4):287–294, 2004.

517 [She94] Jie Shen. Efficient spectral-Galerkin method. I. Direct solvers of
 518 second- and fourth-order equations using Legendre polynomials.
 519 *SIAM J. Sci. Comput.*, 15(6):1489–1505, 1994.

520 [STW11] Jie Shen, Tao Tang, and Li-Lian Wang. *Spectral methods*,
521 volume 41 of *Springer Series in Computational Mathematics*.
522 Springer, Heidelberg, 2011. Algorithms, analysis and applica-
523 tions.

524 [XBKB99] H. Xu, E. Bjerneld, M. Käll, and L. Börjesson. Spectroscopy of
525 single hemoglobin molecules by surface enhanced raman scatter-
526 ing. *Phys. Rev. Lett.*, 83:4357–4360, 1999.